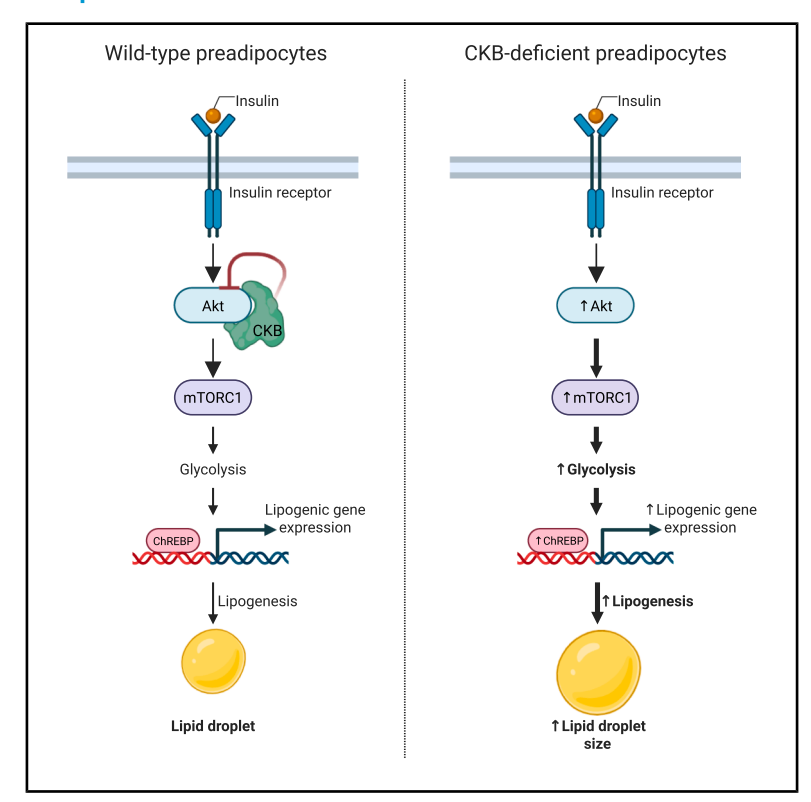
Creatine kinase B regulates glycolysis and de novo lipogenesis pathways to control lipid accumulation during adipogenesis

Graphical abstract



Authors

Gianluca Renzi, Romane Higos, Ivan Vlassakev, ..., Janane F. Rahbani, Simon Lecoutre, Salwan Magdasy

Correspondence

simon.lecoutre@inserm.fr (S.L.), salwan.maqdasy@ki.se (S.M.)

In brief

Renzi et al. identify creatine kinase B (CKB) as a metabolic sensor during white adipocyte differentiation. By modulating AKT, CKB fine-tunes insulin signaling and glycolysis to restrain ChREBP activation, thereby controlling *de novo* lipogenesis. This work links creatine metabolism to nutrient-responsive transcriptional regulation of lipid accumulation.

Highlights

- CKB and CKMT2 are progressively upregulated during white adipocyte differentiation
- Loss of CKB increases glycolytic flux, fueling glucose-driven lipid synthesis via ChREBP
- CKB fine-tunes AKT activity and modulates insulinstimulated AKT-mTORC1 signaling







Report

Creatine kinase B regulates glycolysis and de novo lipogenesis pathways to control lipid accumulation during adipogenesis

Gianluca Renzi,¹ Romane Higos,^{1,2} Ivan Vlassakev,¹ Abdoul Akim Bello,³ Muhmmad Omar-Hmeadi,⁴ Mattias Hansen,¹ Fatiha Merabtene,² Christine Rouault,² Ondrej Hodek,⁵ Lucas Massier,^{1,6} Bruno Antonny,³ Geneviève Marcelin,² Janane F. Rahbani,⁷ Simon Lecoutre,^{2,9,*} and Salwan Maqdasy^{1,8,9,10,*}

SUMMARY

White adipocyte differentiation or adipogenesis requires coordination of metabolic sensing and transcriptional modifications to orchestrate lipid storage. Creatine and its kinases are implicated in adipose energy buffering, but the roles of cytosolic (CKB) and mitochondrial (CKMT2) creatine kinases in adipogenesis are unclear. We find that both CKB and CKMT2 are progressively upregulated during differentiation. Functional studies show that CKB restrains *de novo* lipogenesis (DNL) by limiting activation of carbohydrate-responsive element-binding protein (ChREBP), a key regulator of lipogenic genes. Mechanistically, CKB interacts with AKT and regulates its activation in response to insulin. Loss of CKB causes persistent AKT-mTORC1 signaling, increases glycolytic flux, and enhances ChREBP activation, thereby promoting glucose-derived lipid synthesis. Thus, CKB acts as a metabolic rheostat linking creatine-kinase activity to insulin signaling and nutrient-responsive transcription. We propose a CKB-AKT-ChREBP regulatory axis that contributes to metabolic remodeling and lipid homeostasis during adipocyte differentiation.

INTRODUCTION

Lipid turnover is essential for maintaining metabolic homeostasis, allowing white adipose tissue (WAT) to safely store excess nutrients during periods of energy surplus. However, under chronic overnutrition, sustained lipid accumulation in WAT and the liver promotes lipotoxicity, driving insulin resistance and the development of type 2 diabetes (T2D). To mitigate this, lipid synthesis and storage are tightly regulated across tissues, with WAT and the liver serving as the primary lipogenic organs. WAT adapts by expanding through hypertrophy of existing adipocytes and through adipogenesis from resident precursors, processes essential for preserving adipose plasticity and mitigating ectopic lipid deposition. Disruption of these adaptive responses underlies the progression of cardiometabolic disease.

Adipogenesis is orchestrated by a well-defined transcriptional cascade involving the sequential activation of early (C/EBP β ,

C/EBP δ , glucocorticoid receptor, CREB) and late (C/EBP α , PPARy) regulators that establish and maintain adipocyte identity. 7,9,10 While these transcriptional mechanisms are well characterized, the metabolic remodeling that fuels adipogenesis and supports lipid accumulation in vivo remains poorly understood. A central metabolic pathway in this process is de novo lipogenesis (DNL), which converts carbohydrate-derived acetyl-CoA into fatty acids. 11 In differentiating human adipocytes, DNL can supply the full complement of fatty acids required for maturation. 12 Indeed, fetal human adipocytes exhibit high lipogenic capacity as they develop into mature fat cells, ¹³ and *in vitro*, human preadipocytes can fully differentiate and accumulate lipid droplets even in the absence of an exogenous fat source. 14 Although the liver is the major site of systemic lipid synthesis, adipose DNL plays a distinct and protective role by channeling potentially toxic sugars into inert lipid stores, thereby buffering metabolic stress.1



¹Department of Medicine (H7), Karolinska Institutet, ME Endokrinologi, Karolinska University Hospital Huddinge, Huddinge 141 83, Sweden

²Nutrition and Obesities: Systemic Approaches Research Group (Nutri-Omics), Sorbonne Université, INSERM, Paris 75013, France

³Université Côte d'Azur, CNRS and Inserm, Institut de Pharmacologie Moléculaire et Cellulaire, UMR 7275, Sophia Antipolis, France

⁴Department of Animal Biosciences, Swedish University of Agricultural Sciences, Uppsala, Sweden ⁵Swedish Metabolomics Center, Department of Forest Genetics and Plant Physiology, Swedish University of Agricultural Sciences, Umeå,

Sweden

6Helmholtz Institute for Metabolic, Obesity and Vascular Research (HI-MAG) of the Helmholtz Zentrum München at the University of Leipzig

and University Hospital Leipzig, Leipzig, Germany

7Section of Hematology and Oncology, Department of Medicine, The University of Chicago, Chicago, IL 60637, USA

⁸ANOVA, Karolinska University Hospital, Stockholm, Sweden

⁹These authors contributed equally

¹⁰Lead contact

^{*}Correspondence: simon.lecoutre@inserm.fr (S.L.), salwan.maqdasy@ki.se (S.M.) https://doi.org/10.1016/j.celrep.2025.116489



Paradoxically, DNL has shown tissue-specific associations with metabolic disease: it is positively correlated with insulin resistance in the liver but negatively correlated in adipose tissue. 11,15,16 In both obese mice and individuals with obesity, DNL flux in WAT is often suppressed, suggesting a link to insulin sensitivity. 17 Despite this clinical relevance, the molecular and metabolic mechanisms that regulate DNL during adipogenesis remain incompletely defined. Recent studies have suggested that amino acid metabolism may support lipid anabolism during adipocyte differentiation; however, whether additional energetic pathways contribute to this process is still unclear. 18–20

Using integrated transcriptomic and proteomic analyses, we identified significant changes in the creatine kinase system during adipogenesis. Creatine functions as a cellular energy buffer through the action of mitochondrial CKMT2 and cytosolic creatine kinase B (CKB), which shuttle high-energy phosphate groups between subcellular compartments. While prior studies have linked creatine and CKB to mitochondrial activity, thermogenesis, whole-body energy expenditure and inflammation, 22-26 their role in white adipocyte differentiation and lipogenesis has remained undefined.

Here, we demonstrated that CKB acts as a metabolic gate-keeper of lipogenesis during adipogenesis. We found that CKB is as a key regulator of adipogenesis, insulin signaling, and fat storage via DNL. By fine-tuning insulin-mediated AKT pathway activation, CKB helps control the balance between anabolic signaling and lipid synthesis. Loss of CKB led to sustained AKT-mTORC1 activity, enhanced glycolysis, and increased carbohydrate-responsive element-binding protein (ChREBP)-driven transcription of lipogenic genes, thereby fueling DNL. These results reveal a novel CKB-AKT-ChREBP axis linking creatine metabolism to insulin-dependent lipogenesis. Together with recent studies on CKB's role in regulating fat cell bioenergetic and inflammatory status, ^{22,23,26} our findings position CKB as a metabolic gatekeeper of adipose tissue function and systemic metabolism.

RESULTS

Temporal induction of creatine kinases reflects metabolic reprogramming during adipogenesis

To investigate metabolic reprogramming during human adipogenesis, we analyzed time-resolved transcriptomic data from the FANTOM5 consortium, 27 capturing the differentiation of our in vitro differentiating human preadipocytes from day 0 (D0) to fully mature adipocytes at D12. At each time point, we identified significantly enriched pathways and visualized them as an interconnected network of metabolic processes. This revealed extensive remodeling of cellular metabolism at the end of differentiation (Figure 1A), with amino acid-related pathways being particularly enriched. Among these, the arginine-proline metabolism pathway displayed one of the strongest inductions in expression throughout adipogenesis (Figure S1A). This finding aligns with emerging research highlighting amino acid metabolism as a critical regulator in adipocyte differentiation and function. 18,19,28-30 Within this pathway, CKB and CKMT2, encoding cytosolic and mitochondrial creatine kinases, respectively, stood out among the most upregulated genes throughout adipogenesis

(Figures 1B and S1B). Both western blotting and LC-MS-based proteomics^{31,32} demonstrated a sustained increase in CKB and CKMT2 expression at the protein level across the course of differentiation (Figures 1C and 1D).

Notably, the expression of both cytosolic CKB and mitochondrial CKMT2 was markedly upregulated only during the late phase of adipocyte differentiation, becoming prominent after D5 (Figure 1D). Prior studies have established that triiodothyronine (T₃) enhances creatine kinase expression and activity in high-energy-demand tissues such as cardiac and skeletal muscle.³⁴ Given that T₃ is a component of the adipogenic differentiation cocktail used in human preadipocyte cultures, we investigated whether thyroid hormone directly contributes to creatine kinase regulation during adipogenesis. Individual components of the differentiation cocktail were sequentially omitted between D5 and D8. While removal of the PPARy agonist had no discernible effect, the omission of T₃ revealed a specific requirement for thyroid hormone in driving creatine kinase expression (Figure S1C). To directly assess responsiveness to thyroid hormone, differentiating adipocytes were deprived of the full differentiation cocktail from D5 to D8 and subsequently acutely stimulated with T3. This brief exposure was sufficient to robustly induce CKB and CKMT2 mRNA expression (Figure 1E). Notably, this induction coincided with enrichment of thyroid hormone signaling signatures, consistent with the inclusion of T3 as a key component of the adipogenic cocktail. In line with these observations, motif enrichment analysis identified multiple thyroid hormone receptor (THR) binding sites within regulatory regions proximal to the CKB and CKMT2 loci (Figure S1D).

Our *in vitro* findings were corroborated by spatial transcriptomic profiling of human WAT, ^{32,33} which showed that *CKB* and *CKMT2* expression is predominantly enriched in mature adipocytes, with fewer expression in preadipocytes (Figure 1F). Further validation using qPCR on isolated cells from human subcutaneous WAT biopsies confirmed significantly higher expression of *CKB* and *CKMT2* in mature adipocytes compared to preadipocytes (Figure 1G). In summary, these findings identify CKB and CKMT2 as key T3-responsive metabolic genes that are robustly induced during human adipogenesis.

Silencing of CKB enhances triglyceride accumulation via DNL without altering adipogenesis

To determine the functional role of creatine kinase activity during human adipogenesis, we selectively silenced CKB and CKMT2 in primary human preadipocytes using lipid nanoparticle-delivered small interfering RNAs (siC, siCKB, and siCKMT2). This approach achieved robust knockdown of both mRNA and protein levels throughout the differentiation process (Figures 2A and 2B). Surprisingly, loss of either CKB or CKMT2 did not impair adipocyte differentiation, as the expression of key adipogenic markers, including ADIPOQ (adiponectin) and PPARγ, remained unchanged at both mRNA and protein levels (Figures 2B and S2A-S2C). However, CKB depletion markedly increased intracellular lipid accumulation, as shown by enhanced BODIPY intensity and lipid droplet area per adipocyte. This was accompanied by excessive triglyceride (TG) accumulation in siCKB cells, whereas CKMT2 knockdown had no such effect (Figures 2C and 2D). This suggests a selective role for cytosolic creatine kinase in

Report



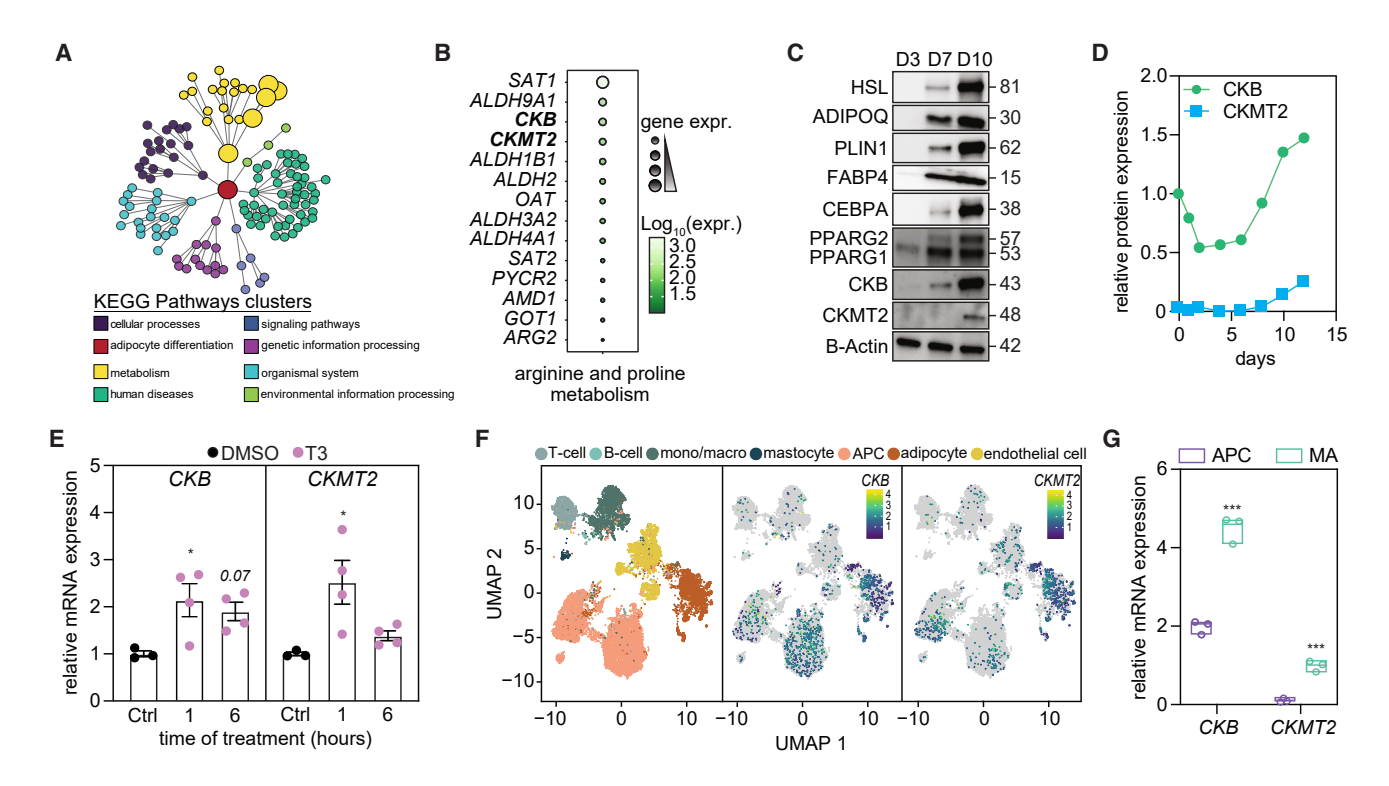


Figure 1. Temporal induction of creatine kinases reflects metabolic reprogramming during adipogenesis

(A) KEGG enrichment analysis of all significantly enriched pathways at day 12 (D12) of *in vitro* human white preadipocyte differentiation (FANTOM5 dataset), 27 with pathways clustered into functional superfamilies. Color-coding legend is shown below the plot.

(B) Gene expression ranking of all the genes upregulated in "arginine and proline metabolism" KEGG pathway at D12 of differentiation. Gene name is specified on the left. Size and color of the dots are related to gene expression.

(C) Representative immunoblot of differentiating *in vitro* human white preadipocytes at D3, D7, and D10 of differentiation, demonstrating progressive upregulation of creatine kinases and adipogenic markers during adipogenesis.

(D) Proteomics analysis of differentiating human white preadipocytes from D0 (start of differentiation) to D12, showing temporal expression patterns of CKB and CKMT2.³¹ Values are mean expressions for each time point.

(E) Relative mRNA expression of CKB and CKMT2 in cells cultured without adipogenic cocktail from D5 to D8, followed by acute stimulation with triiodothyronine (T3) for 1 or 6 h. Data are presented as mean \pm SEM. Statistical significance was determined using one-way ANOVA followed by Dunnett's multiple-comparison test. *p < 0.05 vs. control (DMSO, no T3 treatment).

(F) UMAPs plots of human white adipose tissue single-nucleus transcriptomes; on the left, representation of each cell type in relation to clusters (color coded, legend above the plot); on the center and left, expression of CKB and CKMT2, respectively. 32,33

(G) Relative mRNA expression of CKB and CKMT2 in white adipose tissue fractions isolated from human biopsies—adipose precursor cells (APCs) and mature adipocytes (MAs). Values are presented as min-max. p value was calculated by Student's t-test. ***p < 0.001.

limiting lipid storage capacity. The link between CKB and lipid accumulation was corroborated in human adipose tissue, where *CKB* (but not *CKMT2*) mRNA levels negatively correlated with adipocyte cell volume, even after adjusting for body mass index (BMI; Figure 2E).

To explore the molecular mechanisms underpinning this phenotype, we performed RNA-seq on siCKB, siCKMT2, and control adipocytes. Principal component analysis (PCA) revealed distinct transcriptional signatures for each condition (Figure S2D), and knockdown efficiency was confirmed (Figure S2E). While adipogenic gene networks remained largely intact, siCKB but not siCKMT2 cells exhibited marked upregulation of DNL-associated pathways (Figures 2F and S2F). Indeed, the expression of genes encoding key DNL enzymes was increased only in siCKB cells compared to both controls and siCKMT2 (Figure 2G). This transcriptional reprogramming translated into functional changes in lipid metabolism. Using

in vitro DNL assays with [³H]-glucose incorporation into TG, we observed a marked increase in insulin-stimulated lipogenesis in siCKB cells (Figure 2H). Consistently, intracellular palmitate levels, one of the major products of DNL, were elevated in siCKB cells (Figure 2I), establishing a link between CKB suppression and enhanced TG accumulation through DNL.

To further test this relationship, we overexpressed CKB (*CKB*^{oe}) using a dCas9-VPR activation system prior to induction of adipogenesis. While CKB^{oe} did not alter adipogenic markers (Figure 2J), it suppressed DNL gene expression and significantly reduced lipid accumulation in mature adipocytes (Figures 2K, 2L, and S2G).

To explore the *in vivo* relevance of these findings, we analyzed adipocyte-specific *Ckb* knockout mice (*Ckb*^{AdipoCre})²² and challenged them with a high-fat diet (HFD) for 6 weeks. These mice exhibited marked induction in the expression of DNL-associated genes in inguinal WAT with preserved expression of mature



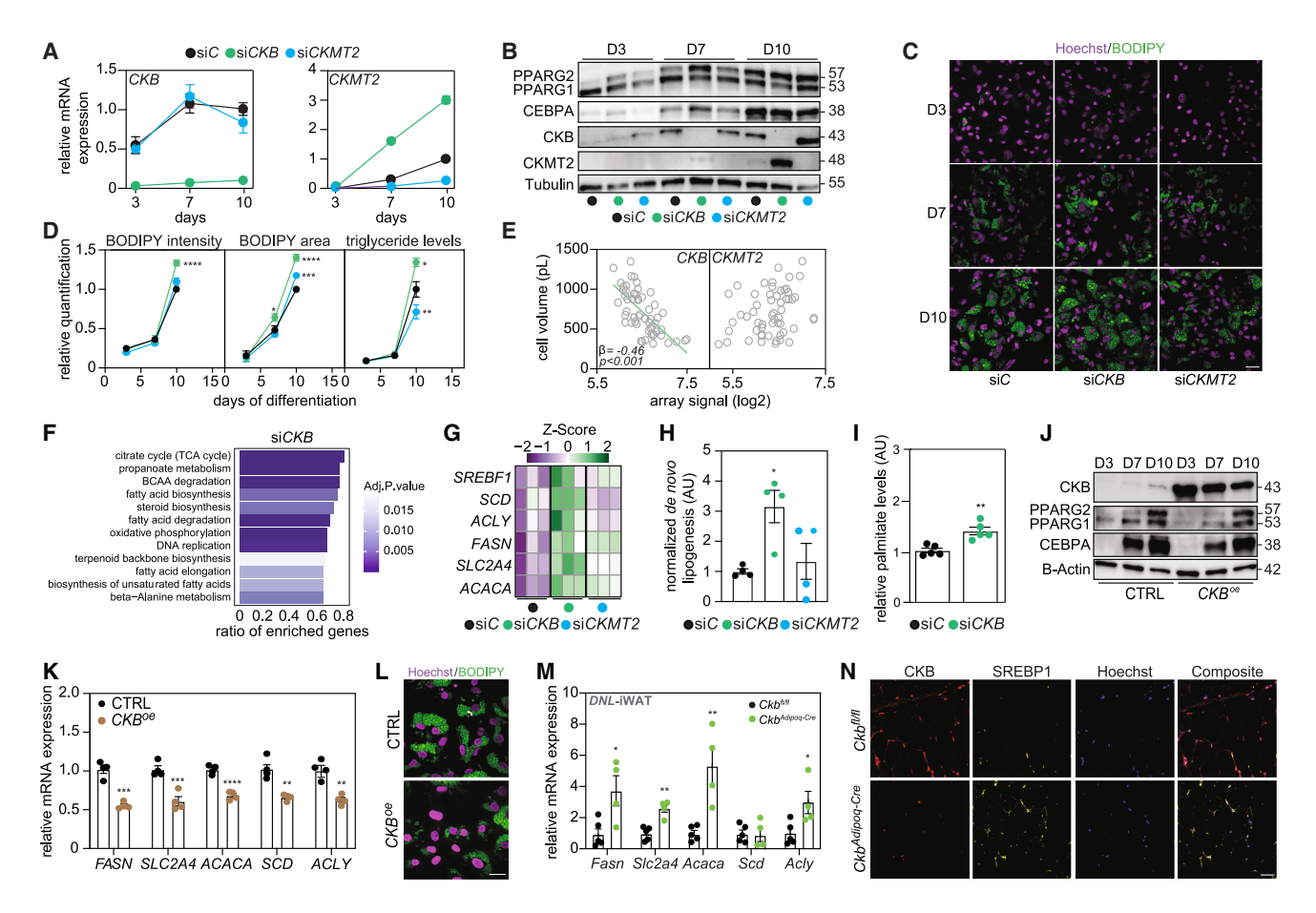


Figure 2. Silencing of creatine kinase B enhances triglyceride accumulation via de novo lipogenesis without altering adipogenesis

(A) Relative mRNA expression of CKB and CKMT2 in differentiating human white preadipocytes transfected at day -1 (D-1; 24 h before induction of differentiation) with non-silencing control (siC), CKB-targeting (siCKB), or CKMT2-targeting (siCKMT2) siRNA. Cells were collected at D3, D7, and D10 of differentiation for analysis. Data are presented as mean ± SEM.

- (B) Representative immunoblot of differentiating in vitro human white preadipocytes transfected with siC, siCKB, or siCKMT2 at D-1. Cells were lysed at D3, D7, and D10 for analyses.
- (C) Representative immunohistochemical staining for Hoechst (nuclei) and BODIPY (lipid droplets) in human white preadipocytes transfected with siC, siCKB, or siCKMT2 24 h before induction of differentiation (D-1). Cells were fixed for staining at D3, D7, and D10 of differentiation. Scale bar represents 20 μm.
- (D) Quantification of BODIPY intensity per cell on the left, BODIPY area per cell on the center, and triglycerides content (measured by triglyceride quantification kit) on the right. siC-, siCKB-, and siCKMT2-transfected cells were analyzed at D3, D7, and D10 of differentiation. BODIPY values were normalized to Hoechst signal; triglycerides were normalized to total protein content. Values are mean \pm SEM. p value was calculated by two-way ANOVA and Tukey's multiple-comparison test, n > 10, *p < 0.05, **p < 0.01, ***p < 0.001, ****p < 0.001
- (E) Correlation between *CKB* (left) or *CKMT2* (right) mRNA expression and cell volume in human subcutaneous white adipose tissue from subjects with obesity (OB, n = 30) or without obesity (NO, n = 26). Statistical significance was determined by Spearman correlation; standardized β values were calculated with p values adjusted for body mass index (BMI).
- (F) KEGG pathways enriched in siCKB cells compared to siC; color represents significance of enrichment, and on the x axis is displayed the enrichment ratio of genes/tot gene ontologies.
- (G) Heatmap representing the expression of genes involved for *de novo* lipogenesis (DNL) in cells transfected with siC, siCKB, or siCKMT2 at D-1 and lysed for analyses at D10 of differentiation. Values are row centered and scaled.
- (H) Stimulated DNL in human white preadipocytes transfected at D-1 with siC, siCKB, or siCKMT2 and harvested at D10 of differentiation. Values were normalized to total protein content and are presented as mean \pm SEM. Statistical significance was assessed by one-way ANOVA with Dunnett's multiple-comparison test vs. siC. *p < 0.05.
- (I) Targeted metabolomic level of intracellular palmitate in human white preadipocytes transfected with siC or siCKB at D-1 and lysed for analyses at D10 of differentiation. Values are mean ± SEM. p value was calculated by Student's t-test, **p < 0.01.
- (J) Representative immunoblot of differentiating human white preadipocytes transfected at D-1 with mRNA encoding catalytically inactive Cas9 coupled to a VPR complex with or without guide RNAs (gRNAs) targeting the CKB promoter, harvested at D3, D7, and D10 of differentiation.
- (K) Relative mRNA expression of DNL-related genes of differentiating human white preadipocytes transfected with mRNA encoding catalytically inactive Cas9 coupled to a VPR complex with or without guide RNA targeting CKB promoter and harvested at D10 of differentiation. Values are mean \pm SEM. p value was calculated by Student's t test, **p < 0.01, ***p < 0.001, ****p < 0.0001.

(legend continued on next page)

Report



adipocyte markers (Figures 2M and S2H), while this effect was absent in the epididymal depot (Figure S2I). Immunofluorescence analysis revealed elevated levels of SREBP1, one of DNL markers, supporting CKB's repressive role *in vivo* (Figures 2N and S2J).

To independently validate the link between CKB and DNL, we employed multiple complementary strategies. First, to pinpoint the critical window of CKB's influence on DNL, we temporally knocked down CKB at D3 and D8 of differentiation. Early knockdown (D3) recapitulated the effects on DNL gene induction (Figure S2K), whereas late knockdown (D8) failed to induce DNL genes (Figure S2L), suggesting a temporal window during early differentiation where CKB modulates lipogenesis. Second, CKB knockdown replicated the pro-lipogenic phenotype across distinct preadipocyte models, including female-donor-derived human white preadipocytes, human adipose-derived stem (hMADS) cells,³⁶ and primary murine preadipocytes isolated from inguinal WAT of female mice, demonstrating conserved regulation of DNL (Figures S2M-S2O). Finally, CRISPR-Cas9mediated CKB knockout in in vitro human white preadipocytes recapitulated the phenotype, excluding potential off-target effects of siRNA-based silencing (Figure S2P).

Collectively, these findings position the cytosolic CKB as a regulator of adipocyte lipid storage and a molecular fine-tuner on DNL during human adipogenesis.

CKB depletion drives ChREBP-mediated lipogenesis through enhanced glycolytic flux

Given that glucose is the primary carbon source for DNL, 11 we first assessed glucose uptake in adipocytes lacking CKB. The expression of SLC2A4, which encodes the insulin-responsive glucose transporter GLUT4, was significantly increased in siCKB adipocytes (Figure 2G), indicating enhanced glucose influx in the absence of CKB. Based on this observation, and on prior evidence linking glycolysis to lipogenesis, 11,37 we hypothesized that CKB depletion promotes glycolytic flux, thereby fueling DNL. To test this, we measured glycolytic activity on D10 of differentiation using Seahorse extracellular flux analysis. siCKB adipocytes exhibited a pronounced increase in extracellular acidification rate (ECAR; Figure 3A), consistent with elevated glycolytic throughput. Concurrently, intracellular ATP levels were significantly elevated (Figure S3A), while oxygen consumption rate (OCR) remained unchanged (Figure S3B), suggesting that metabolic reprogramming was specific to glycolysis rather than mitochondrial oxidative phosphorylation. To evaluate whether this increase in glycolysis supplies precursors for lipogenesis, we performed targeted metabolomic profiling. This revealed substantial accumulation of glycolysis-related intermediates, including fructose-6-phosphate (F6P), xylulose-5-phosphate (X5P), pyruvate, and lactate (Figure 3B), which can contribute to fatty acid synthesis.38 We also observed elevated succinate levels, a tricarboxylic acid (TCA) cycle intermediate that could support lipogenesis through citrate production¹⁷ (Figure S3C).

The elevation of X5P in siCKB adipocytes prompted us to examine the activation of ChREBP, a central transcriptional regulator of DNL that is thought to be stimulated by glycolysisderived sugar phosphates such as X5P.38 ChREBP, encoded by the MLXIPL gene, exists as a glucose-sensitive full-length isoform (~100 kDa) with modest activity, and a shorter, transcriptionally potent isoform (~35 kDa) induced by glycolytic flux.^{39–41} Lacking the N-terminal low-glucose inhibitory domain (LID), the truncated isoform localizes constitutively to the nucleus and is \sim 20-fold more active. Together, these isoforms create a feedforward circuit in which elevated glucose promotes its own conversion into lipids. 39-41 Strikingly, siCKB adipocytes showed a sharp rise in the active 35 kDa ChREBP isoform (Figures 3C and S3D). To functionally test the requirement for ChREBP in mediating this phenotype, we silenced MLXIPL in siCKB adipocytes at D8 of differentiation. MLXIPL knockdown efficiently suppressed ChREBP protein expression (Figure 3D) and completely abrogated the induction of DNL target genes and lipid accumulation observed in CKB-deficient cells (Figures 3E and 3F). These findings support a model in which ChREBP acts as a downstream effector of CKB loss, linking enhanced glycolytic flux and sugar phosphate accumulation to the transcriptional activation of lipogenesis.

To directly test whether glycolytic flux is the upstream driver of ChREBP activation and lipogenesis in *CKB*-deficient adipocytes, we treated si*CKB* cells with 2-deoxy-D-glucose (2-DG), a competitive inhibitor of glycolysis. As expected, 2-DG treatment normalized glucose uptake in si*CKB* adipocytes to levels observed in control cells (Figure 3G) and fully reversed the metabolic reprogramming induced by CKB loss. Specifically, 2-DG abrogated ChREBP protein accumulation, suppressed the expression of ChREBP target genes involved in DNL, and reduced BODIPY intensity per adipocyte (Figures 3H–3J). These results confirm that increased glycolytic flux is required for ChREBP activation and lipogenesis in the absence of CKB. Collectively, our findings define the CKB-glycolysis-ChREBP regulatory axis, which governs lipid biosynthesis in human adipocytes.

CKB depletion is linked to elevated mTORC1 signaling

We next investigated the upstream mechanism by which CKB restrains glycolytic flux. We first evaluated the canonical creatine (Cr)–phosphocreatine (PCr) shuttle. Consistent with impaired cytosolic CKB activity, siCKB adipocytes exhibited a significant increase in the PCr-to-Cr ratio (Figure S4A), indicative of disrupted PCr cycling. However, supplementation with exogenous PCr (1–30 mM) during differentiation reduced *SLC2A4* mRNA expression encoding for GLUT4 but failed to alter the classical

⁽L) Representative images of differentiating human white preadipocytes transfected with mRNA encoding catalytically inactive Cas9 coupled to a VPR complex cells with or without CKB-targeting guide RNAs fixed and stained at D10 of differentiation. Scale bar represents 10 μ m.

⁽M) Relative mRNA expression of DNL-related genes in inguinal white adipose tissue (iWAT) of $Ckb^{fl/fl}$ and $Ckb^{Adipoq-Cre}$ male mice. Values are mean \pm SEM. p value was calculated by Student's t test t = 0.05, t = 0.0

⁽N) Representative immunofluorescent staining of CKB, SREBP1, and Hoechst in paraffin-embedded inguinal WAT (iWAT) from *Ckb*^{#/ff} and *Ckb*^{Adipoq-Cre} male mice. Group is specified on the left of the images and channel on top of them. Scale bar represents 50 μm.



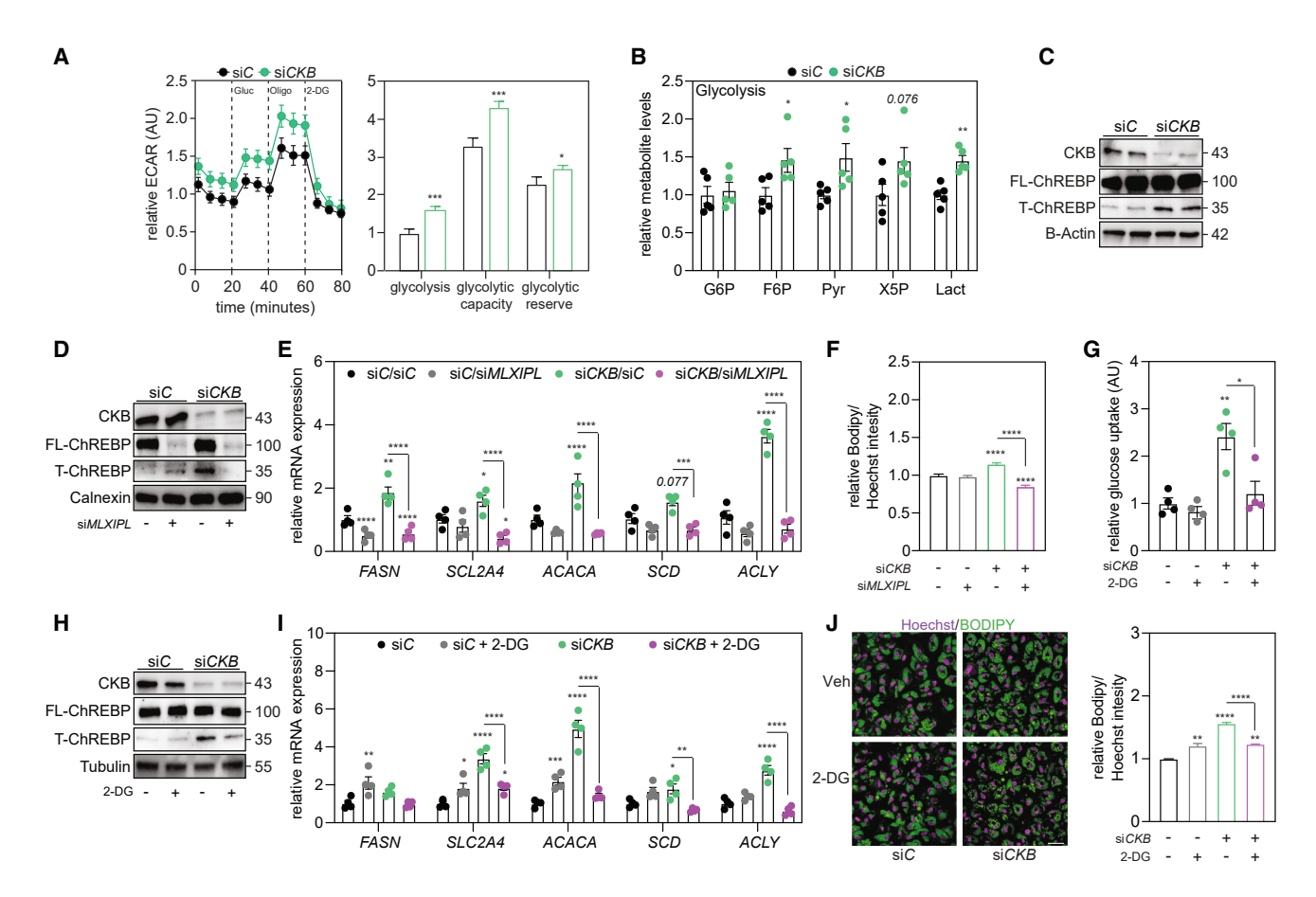


Figure 3. CKB depletion stimulates ChREBP-mediated lipogenesis through enhanced glycolytic flux

(A) On the left: representative Seahorse GlycoStress test analysis of extracellular acidification rate (ECAR) in human preadipocytes transfected at D-1 with siC or siCKB and analyzed after 10 days of differentiation. On the right: ECAR profile over time. Right: quantification of relative glycolysis, glycolytic capacity, and glycolytic reserve. Data are mean \pm SEM. Statistical significance was determined by Student's t test. t 10, t 20.001. Abbreviations: Gluc, glucose; Oligo, oligomycin: 2-DG, 2-deoxy-glucose.

- (B) Targeted metabolite levels related to glycolysis in *in vitro* human white preadipocytes transfected at D-1 with siC or siCKB and harvested at D10 of differentiation for analysis. Data are presented as mean \pm SEM. p value was calculated using Student's t test. p < 0.05, p < 0.01. Abbreviations: G6P, glucose-6-phosphate; F6P, fructose-6-phosphate; X5P, xylulose-5-phosphate; Pyr, pyruvate; Lact, lactate.
- (C) Representative immunoblot of ChREBP isoforms in human preadipocytes transfected at D-1 with control siC or siCKB and harvested at D10 of differentiation. Bands correspond to the full-length isoform (FL) and the truncated, transcriptionally active isoform (T) of ChREBP.
- (D) Representative immunoblot of cells transfected at D-1 with siC or siCKB and re-transfected at D8 with siC or siMLXIPL (targeting ChREBP expression), confirming ChREBP knockdown at D10 of differentiation. Bands correspond to full-length (FL) and truncated, transcriptionally active (T) isoforms of ChREBP. (E) Relative mRNA expression of DNL-related genes in early siC- and siCKB-transfected cells (transfection at D-1), re-transfected at D8 with siC or siMLXIPL, and harvested for analysis at D10 of differentiation. Values are mean ± SEM. p value was calculated with two-way ANOVA and Tukey's multiple-comparison test, comparing all conditions to siC unless indicated otherwise, *p < 0.05, **p < 0.01, ***p < 0.001, ****p < 0.0001.
- (F) Representative high-throughput quantification of BODIPY staining in early siC- or siCKB-transfected cells (transfected at D-1) re-transfected at D8 with siC or siMLXIPL, and harvested for analysis at D10 of differentiation. BODIPY intensity was normalized to Hoechst signal. Data are mean \pm SEM. Statistical significance was determined by two-way ANOVA with Tukey's multiple-comparison test, comparing all conditions to siC unless indicated otherwise. n > 10, ****p < 0.0001. (G) Representative glucose uptake assay using 2-deoxy-D-[1- 3 H]-glucose in human preadipocytes transfected on D-1 with siC or siCKB. At D10 of differentiation, cells were treated with vehicle or 2-DG for 48 h and then harvested for analysis. Data are presented as mean \pm SEM. p value was calculated using two-way ANOVA and Tukey's multiple-comparison test, comparing all conditions to siC unless indicated otherwise, *p < 0.05, **p < 0.05.
- (H) Representative immunoblot showing ChREBP protein isoforms in cells transfected on D-1 with siC or siCKB. At D10 of differentiation, cells were treated with vehicle or 2-DG for 48 h and then harvested for analysis.
- (l) Relative mRNA expression of DNL-related genes in differentiating human white preadipocytes transfected at D-1 with siC or siCKB, treated D10 of differentiation with vehicle or 2-DG for 48 h, and then harvested for analysis. Data are presented as mean \pm SEM. p value was calculated using two-way ANOVA and Tukey's multiple-comparison test, comparing all conditions to siC unless indicated otherwise, *p < 0.05, **p < 0.01, ***p < 0.001, ****p < 0.0001.
- (J) On the left, representative immunohistochemical of nuclei (Hoechst) and lipid droplets (BODIPY) in cells transfected at D-1 with siC or siCKB, incubated with vehicle or 2-DG for 48 h at D10 of differentiation, and fixed for analysis. Scale bar represents 20 μ m. Right: high-throughput quantification of BODIPY intensity normalized to Hoechst signal. Data are mean \pm SEM. Statistical significance was assessed by two-way ANOVA with Tukey's multiple-comparison test, comparing all conditions to siC unless indicated otherwise. n > 10 per group, **p < 0.01, ****p < 0.0001.

Report



DNL-related gene expression (Figure S4B), effectively excluding a PCr-mediated mechanism.

We next considered AMP-activated protein kinase (AMPK), a master energy sensor regulated by intracellular ATP levels and creatine metabolism, ^{26,43} and a well-established suppressor of DNL. ⁴⁴ In line with the observed increase in ATP levels (Figure S3A), CKB-depleted adipocytes exhibited reduced AMPK activity (based on phosphorylation of threonine 172; Figures 4A and S4C). However, pharmacological activation of AMPK using PF-739 induced AMPK phosphorylation but failed to totally reverse DNL-related gene expression in si*CKB* cells (Figures 4A and 4B).

Given prior evidence that creatine metabolism modulates mTORC1 signaling in other cell types, 45 we next investigated whether mTORC1 drives the ChREBP-dependent DNL observed upon CKB knockdown during human adipogenesis. Indeed, mTORC1 is a central nutrient- and energy-sensing kinase complex known to orchestrate anabolic programs such as glycolysis and lipogenesis. 46 CKB knockdown led to increased phosphorylation of P70S6K, a downstream target of mTORC1, indicative of enhanced mTORC1 activity (Figures 4C and S4C). To determine the functional relevance of this pathway, we treated siCKB adipocytes with rapamycin, a selective mTORC1 inhibitor. 47,48 Rapamycin treatment markedly reduced P70S6K phosphorylation, DNL-related gene expression, and lipid accumulation in siCKB cells compared to controls (Figures 4C-4E). establishing mTORC1 as a key mediator of the metabolic and lipogenic effects observed upon CKB depletion. Importantly, this regulatory role is independent of CKB's canonical function within the PCr energy shuttle, revealing a non-canonical mechanism by which CKB modulates energy sensing and lipid metabolism in adipocytes.

CKB regulates DNL via AKT fine-tuning

We next investigated the upstream mechanism by which CKB controls mTORC1 activation in adipocytes. We first assessed the potential role of branched-chain amino acids (BCAAs), known activators of mTORC1.⁴⁹ However, varying extracellular BCAA concentrations across a physiological range during human adipogenesis had no effect on mTORC1 activity nor on DNL gene expression in siCKB adipocytes (Figures S4D and S4E), indicating that CKB regulates mTORC1 independently of BCAA signaling.

We then turned to the PI3K-AKT pathway, a central upstream regulator of mTORC1 and a key mediator of insulin-stimulated glucose metabolism in adipocytes. AKT is not only a well-established activator of mTORC1 but also listed as a potential CKB interactor in the NCBI Gene database. Notably, previous studies have demonstrated CKB-AKT co-immunoprecipitation in both neuronal and cancer cell contexts, 51,52 providing strong rationale for investigating this interaction in adipocytes. Immunoprecipitation of AKT in our human adipocyte model confirmed a physical association with CKB (Figure 4F), supporting the relevance of this interaction in the context of adipogenesis. Furthermore, *CKB* knockdown markedly increased AKT phosphorylation (Figure S4F), a reliable marker for the AKT protein kinase activity. To determine whether AKT activity is required for the lipogenic phenotype observed upon CKB deple-

tion, we treated siCKB adipocytes with MK-2206, a selective allosteric AKT inhibitor. ⁵³ As a parallel control, we deprived adipocytes from insulin to inhibit AKT activation. ⁵⁴ Interestingly, AKT-mTORC1-ChREBP activation is lost in siCKB cells in the absence of insulin (Figure 4G). Moreover, MK-2206 treatment fully abrogated the increase in P70S6K phosphorylation and ChREBP protein accumulation and significantly suppressed DNL-related gene expression, DNL process, and lipid accumulation in siCKB cells (Figures 4G–4J). These findings establish AKT as a key mediator of the metabolic reprogramming observed upon CKB depletion. Supporting this, insulin starvation and restimulation experiments showed that DNL-related gene overexpression in siCKB cells was normalized under insulin deprivation and fully restored following insulin reintroduction (Figure S4G), confirming that the lipogenic response is insulin dependent.

To confirm the specificity of this pathway, we re-expressed *CKB* at D8 in si*C* and si*CKB* adipocytes. *CKB* re-expression was confirmed at both the mRNA and protein levels (Figures 4K and S4H) and functionally reversed the elevated AKT phosphorylation and ChREBP protein accumulation (Figure 4K). This intervention fully rescued the lipogenic phenotype (Figures 4L and 4M), conclusively identifying CKB as a gatekeeper of TG accumulation during human adipogenesis. Finally, time-course analysis during differentiation revealed that CKB depletion initiates a cascade beginning with AKT phosphorylation, followed by enhanced glycolytic activity (measured by ECAR) and increased lactate production (Figures S4I–S4K).

Together, these findings establish CKB as an important regulator that sequesters AKT to limit insulin signaling and tamper DNL via AKT-mTORC1-ChREBP.

DISCUSSION

WAT acts as a dynamic metabolic organ that governs energy storage and mobilization in response to nutrient availability.² Processes such as adipocyte differentiation. WAT expansion, and fat storage are tightly linked to metabolic sequelae. 6,55 However, the precise molecular mechanisms that connect nutrient sensing to metabolic reprogramming, particularly the transcriptional control of lipid accumulation during adipogenesis, remain incompletely defined. Adipogenesis involves a coordinated series of transcriptional and metabolic events that enable preadipocytes to acquire the capacity to store TGs, a critical adaptation that buffers excess energy and preserves systemic metabolic homeostasis.^{2,5,6,56} Optimized lipid storage not only prevents lipotoxicity but also supports metabolically healthy WAT expansion. 2,5,6 Although DNL contributes modestly to TG stores in mature adipocytes in vivo, it plays an essential role during differentiation by facilitating adipocyte maturation, enhancing lipid-buffering capacity, and promoting insulin sensitivity. 12,17,37,57 Conversely, in hepatocytes, DNL drives metabolic dysfunction-associated steatotic liver disease. 15 The contribution of creatine kinases to these processes has been poorly characterized, though creatine supplementation has been shown to mitigate hepatic steatosis in rodent models, 58,59 suggesting a possible metabolic link between creatine metabolism and lipogenesis.

Here, we identify CKB as a non-canonical regulator of lipogenesis during adipogenesis. CKB expression increases



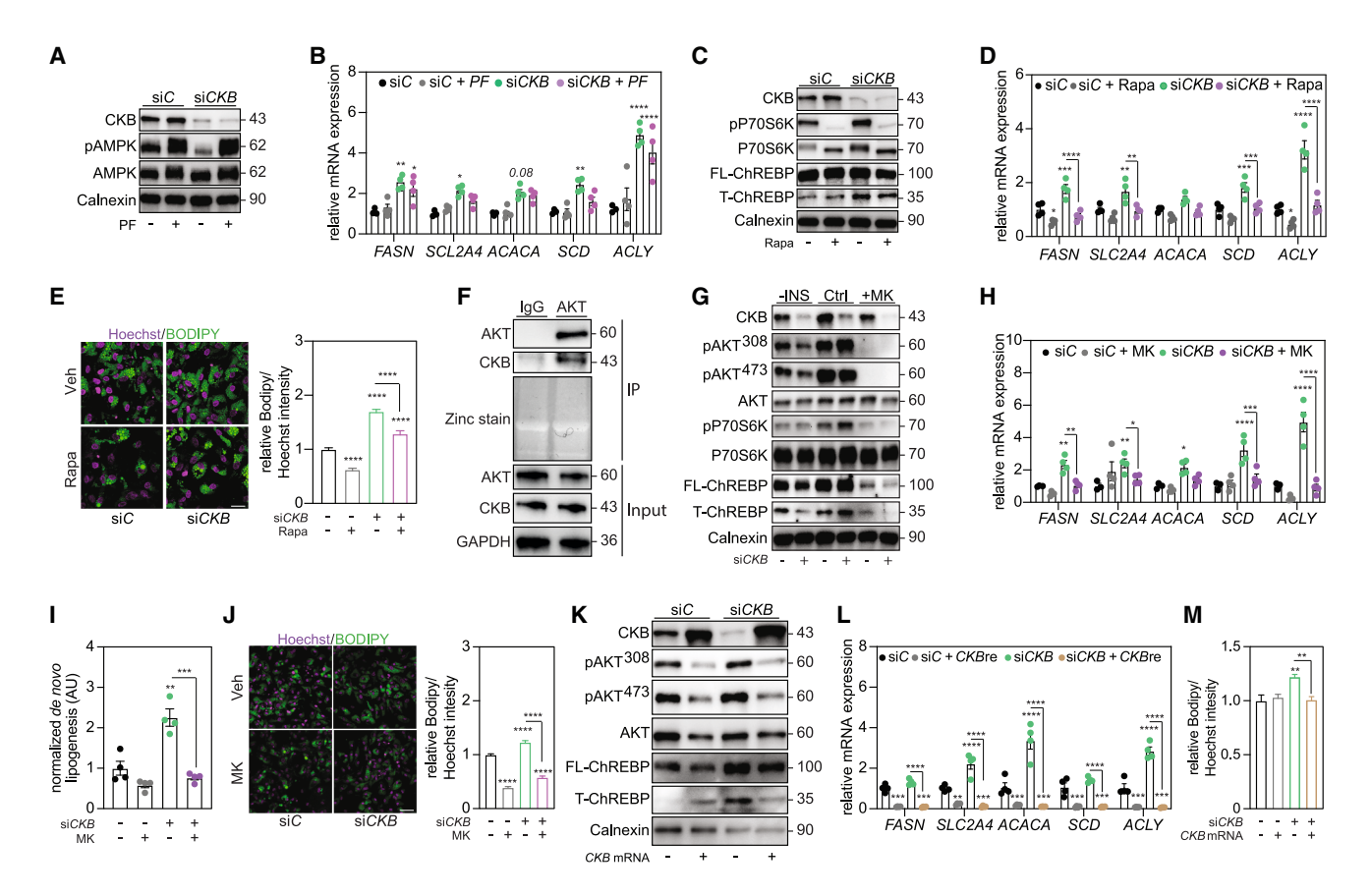


Figure 4. CKB modulates DNL by regulating AKT phosphorylation

(A) Representative immunoblot of cells transfected at D-1 with siC or siCKB. At D10 of differentiation, cells were treated with vehicle or PF-739 for 48 h and then harvested for analysis. The blot shows restored AMPK phosphorylation in siCKB cells following PF-739 treatment.

- (B) Relative mRNA expression of DNL-related genes in human preadipocytes transfected at D-1 with siC or siCKB. At D10 of differentiation, cells were treated with vehicle or PF-739 for 48 h and then harvested for analysis. Data are mean \pm SEM. Statistical significance was assessed by two-way ANOVA with Tukey's multiple-comparison test vs. siC. *p < 0.05, *p < 0.01, ****p < 0.001.
- (C) Representative immunoblot of cells transfected at D-1 with siC or siCKB, incubated with vehicle or rapamycin for 48 h at D10 of differentiation and harvested afterward for analyses.
- (D) Relative mRNA expression of DNL-related gene expression in human preadipocytes transfected at D-1 with siC or siCKB, incubated with vehicle or rapamycin for 48 h at D10 of differentiation and harvested afterward for analyses. Values are mean \pm SEM. p value was calculated using two-way ANOVA and Tukey's multiple-comparison test, comparing all conditions to siC unless indicated otherwise. *p < 0.05, **p < 0.01, ***p < 0.001, ***p < 0.0001.
- (E) On the left, representative immunohistochemical high-throughput quantification of cells transfected at D-1 with siC or siCKB, incubated with vehicle or rapamycin for 48 h at D10 of differentiation, and fixed afterward for analyses. Scale bar represents 20 μ m. On the right, high-throughput quantification of the immunohistochemical BODIPY intensity. Values are relative to Hoechst intensity and represented as mean \pm SEM. p value was calculated using two-way ANOVA and Tukey's multiple-comparison test, comparing all conditions to siC unless indicated otherwise. n > 10 per group, ****p < 0.0001.
- (F) Representative immunoblot of immunoprecipitation of endogenous AKT from whole-cell lysates using AKT antibody or IgG control (upper blot), with corresponding input samples shown (lower blot).
- (G) Representative immunoblot of human preadipocytes transfected at D-1 with siC or siCKB; incubated at D10 of differentiation with vehicle, MK-2206 (Akt inhibitor), or insulin-starved for 48 h (-INS); and harvested afterward for analyses.
- (H) Relative mRNA expression of DNL-related genes in human preadipocytes transfected at D-1 with siC or siCKB, incubated at D10 of differentiation with vehicle or MK-2206 for 48 h, and harvested afterward for analyses. Values are mean \pm SEM. p value was calculated using two-way ANOVA and Tukey's multiple-comparison test, comparing all conditions to siC unless indicated otherwise. *p < 0.05, **p < 0.001, ***p < 0.001, ***p < 0.0001.
- (I) Stimulated DNL assay in cells transfected at D-1 with siC or siCKB, incubated at D10 of differentiation with vehicle or MK-2206 for 48 h, and harvested afterward for analyses. Values are mean \pm SEM. p value was calculated using two-way ANOVA and Tukey's multiple-comparison test, comparing all conditions to siC unless indicated otherwise. **p < 0.01, ***p < 0.001.
- (J) On the left, representative immunohistochemical staining for Hoechst (nuclei) and BODIPY (lipid droplets) in cells transfected at D-1 with siC or siCKB, incubated at D10 of differentiation with vehicle or MK-2206 for 48 h, and fixed afterward for analyses. Scale bar represents 50 μ m. On the right, high-throughput quantification of the immunohistochemical BODIPY intensity. Values are relative to Hoechst intensity and represented as mean \pm SEM. p value was calculated using two-way ANOVA and Tukey's multiple-comparison test, comparing all conditions to siC unless indicated otherwise. n > 10, ****p < 0.0001.
- (K) Representative immunoblot in early siC- and siCKB-transfected cells (transfection at D-1) re-transfected at D8 with either mRNA encoding CKB or a non-coding vehicle.

(legend continued on next page)



progressively during adipocyte differentiation and acts independently of the Cr-PCr energy shuttle to constrain insulin-AKT-mTORC1 signaling. Mechanistically, CKB fine-tunes AKT activity by limiting its phosphorylation, thereby attenuating downstream activation of mTORC1, glycolysis, and ChREBP-driven lipogenesis. Loss of CKB enhances AKT phosphorylation only in the presence of insulin, suggesting that CKB specifically modulates growth factor-driven AKT activation. Whether CKB's enzymatic activity, dictated by its structural conformation, affects AKT binding remains unresolved, as the absence of a selective CKB inhibitor currently limits direct testing of this hypothesis.

Within the broader framework of adipose biology, the AKTmTORC1 axis functions as a central hub for integrating nutrient and growth factor signals, driving both adipogenesis and systemic lipid storage. 60 Pharmacological inhibition of mTORC1 with rapamycin has been shown to impair both adipogenesis and lipogenesis, 61-64 and genetic disruption of its components alters adiposity in vivo. 65,66 A primary upstream activator of mTORC1 is the serine/ threonine kinase AKT, which promotes cell growth and survival by phosphorylating multiple downstream substrates. In adipocytes, AKT stimulates mTORC1 through phosphorylation of the inhibitory regulators TSC2 and PRAS40, thereby promoting lipid biosynthesis and storage. 67 While the activation of AKT via receptor tyrosine kinase-PI3K-mTORC2 pathways is well characterized, the molecular mechanisms that negatively regulate AKT activity are less defined and have been largely attributed to phosphatases such as PTEN and PP2A. 16,68 Our findings extend emerging evidence from T cell biology implicating CKB and creatine metabolism in growth factor-driven anabolic regulation⁴⁵ revealing that, in adipocytes, CKB acts as a protein-based checkpoint that selectively dampens insulin-driven mTORC1 activation, glycolytic flux, and ChREBP-dependent lipogenesis. Mechanistically, our model aligns with oncogenic studies showing that CKB binding can prevent PIP3-dependent AKT activation, 51,52 consistent with our observation that CKB's effects depend on insulin-mediated PI3K activation. 69

In the murine model, adipocyte-specific *Ckb* deletion drives DNL in inguinal WAT while sparing epididymal WAT. We propose that this depot-specific effect reflects differences in inflammatory tone and insulin sensitivity: epididymal WAT is chronically inflamed in obesity, a condition impairing insulin signaling and suppressing DNL, ^{70–73} thereby masking the absence of CKB's fine-tuning effect on AKT. In contrast, inguinal WAT retains relative insulin sensitivity and has a lower inflammatory burden, enabling CKB depletion to directly enhance AKT-mTORC1 activity and lipogenesis, creating a permissive environment in which CKB depletion directly drives lipogenesis. ^{70–73} This model is consistent with human and rodent data linking reduced CKB expression to visceral depot inflammation²⁶ and with reports

that inflammation selectively attenuates DNL in insulin-resistant adipose tissue. ^{17,74} In obesity, CKB downregulation correlates with inflammatory status, ²⁶ and ER stress-driven IRE1-XBP1s signaling has been implicated in DNMT3A-mediated methylation and silencing of the *CKB* promoter. ⁷⁵ We hypothesize that this downregulation may represent a compensatory attempt to boost AKT signaling in the setting of insulin resistance by relieving CKB's inhibitory effect. While such a mechanism could partially restore anabolic signaling, it may also exacerbate adipose dysfunction by amplifying lipogenesis under metabolically unfavorable conditions.

In summary, we identify CKB as a conditional metabolic regulator that integrates nutrient-sensing and insulin signaling pathways to modulate lipogenesis in a depot-specific manner. By directly binding AKT and attenuating insulin-mTORC1-ChREBP signaling, CKB constrains glycolysis and DNL, shaping lipid storage capacity in adipocytes. We propose that CKB functions not as a determinant of differentiation itself but as a metabolic "priming" factor that enables differentiated adipocytes to mount a lipogenic program. Targeting this pathway could allow selective enhancement of lipid storage in metabolically favorable depots while limiting visceral fat accumulation, potentially offering a strategy for improving metabolic health.

Limitations of the study

A limitation of our study is that the full physiological relevance of CKB in murine adipose biology remains incompletely defined. While our data establish a role for CKB in both human and mouse adipocytes and support its in vivo importance, the available mouse model introduces interpretive constraints. Adipocytespecific Ckb deletion predisposes mice to obesity but also impairs glucose homeostasis, a phenotype likely driven by defects in brown adipose tissue thermogenesis and WAT inflammation rather than by isolated changes in lipid metabolism. 22,26 Dissecting CKB's contribution to early adipocyte lineage commitment vs. its function in mature adipocytes will require inducible, progenitor-targeted approaches (e.g., $Pdgfr\alpha^{CreERT2}$), which would clearly separate developmental from maintenance roles. However, Ckb deletion late in differentiation still increases lipogenesis in inguinal WAT. Moreover, targeting Ckb in preadipocytes isolated from murine WAT confirms these findings. Another limitation concerns the depot specificity of the phenotype. Although metabolic and inflammatory differences between adipose depots are well established, the variation in DNL capacity and its regulation across depots remain unclear. Subcutaneous WAT shows higher DNL capacity, which may provide protection against metabolic disorders. 76 This difference may partly reflect the relative enrichment of subcutaneous depots with classical adipocytes, which are specialized in lipid metabolism.⁷⁷ Further studies using adipocytes isolated from each depot are needed to

⁽L) Relative mRNA expression of DNL-related genes in early siC- and siCKB-transfected cells (transfection at D-1) re-transfected at D8 of differentiation with either mRNA encoding CKB or a non-coding vehicle. Values are mean \pm SEM. p value was calculated using two-way ANOVA and Tukey's multiple-comparison test, comparing all conditions to siC unless indicated otherwise. ***p < 0.001, ****p < 0.0001.

⁽M) Representative immunohistochemical high-throughput quantification of early siC- and siCKB-transfected cells (transfection at D-1) re-transfected at D8 of differentiation with either mRNA encoding CKB or a non-coding vehicle. Values are relative to Hoechst intensity and represented as mean \pm SEM. p value was calculated using two-way ANOVA and Tukey's multiple-comparison test, comparing all conditions to siC unless indicated otherwise. n > 10, **p < 0.01.





define the depot-specific roles of creatine metabolism and CKB in adipocyte function.

RESOURCE AVAILABILITY

Lead contact

Requests for further information and resources should be directed to and will be fulfilled by the lead contact Salwan Maqdasy (salwan.maqdasy@ki.se).

Materials availability

This study did not generate new unique reagents.

Data and code availability

- RNA-seq data have been deposited at GEO and are publicly available as of the date of publication (accession GEO: GSE307820).
- This paper does not report original code.
- Additional information is available from the lead contact upon request.

ACKNOWLEDGMENTS

We would like to thank Prof. Mikael Rydén and Dr. Niklas Mejhert for their scientific inputs, supervision, and guidance of this work. Prof. Mikael Rydén designed and supervised the clinical studies where data have been used in this manuscript. We would also like to thank Prof. Karine Clément for her scientific inputs. Additionally, we would like to thank Prof. Martin O. Bergö for allowing us to use the high-resolution respirometry equipment employed in the study. We would like to thank Dr. Lawrence Kazak and Dr. Bozena Samborska who generously provided samples from mice generated at their lab (McGill, Montreal, Canada). We would like to thank Prof. Ez-Zoubir Amri who generously provided hMADS.

Funding sources: S.M. is supported by CIMED, European Foundation for the Study of Diabetes Rising Star award, and Swedish Research Council. S.L. is supported by the French National Agency for Research, ANR-AGAAT, and Association Française d'Étude et de Recherche sur l'obésité (AFERO). B.A. and A.A.B. are supported by the European Research Council (ERC Synergy grant SPHERES # 856404).

AUTHOR CONTRIBUTIONS

Conceptualization, G.R., S.L., and S.M.; methodology, G.R., J.F.R., G.M., B.A., S.L., and S.M.; investigation, G.R., R.H., A.A.B., M.O.-H., I.V., M.H., L.M., F.M., C.R., O.H., J.F.R., S.L., and S.M.; writing – original draft, G.R., S.L., and S.M.; writing – review & editing, G.R., S.L., and S.M.; funding acquisition, S.L. and S.M.; and supervision, S.L. and S.M. All the coauthors read and approved the article.

DECLARATION OF INTERESTS

The authors declare no competing interests.

STAR*METHODS

Detailed methods are provided in the online version of this paper and include the following:

- KEY RESOURCES TABLE
- EXPERIMENTAL MODEL AND SUBJECT DETAILS
 - Subjects
 - Cell cultures
 - o Animals
- METHOD DETAILS
 - $\,\circ\,$ RNA isolation, cDNA synthesis and real-time qPCR
 - o In vitro transcription and mRNA-based re-expression
 - o CRISPRa for endogenous CKB overexpression
 - $\,\circ\,$ RNAi and re-expression experiments at D3 and D8
 - Early transfection of pre-adipocytes (D-1) and incubations with chemicals

- o Library preparation and RNA sequencing
- Western Blot analysis
- o Immunoprecipitation from whole lysate
- o ATP measurement
- Metabolomic samples preparation and targeted metabolomic measurements
- o Creatine kinase activity
- o ELISA assays
- o Triglyceride extraction and measurement
- o Immunofluorescence (IF)
- Confocal microscopy
- o Quantification of lipid accumulation (by Bodipy staining)
- Seahorse assays
- O Radioactive de novo lipogenesis measurement
- o Radioactive glucose uptake measurement
- QUANTIFICATION AND STATISTICAL ANALYSIS

SUPPLEMENTAL INFORMATION

Supplemental information can be found online at https://doi.org/10.1016/j.ceirep.2025.116489.

Received: November 8, 2024 Revised: August 21, 2025 Accepted: October 6, 2025

REFERENCES

- Olzmann, J.A., and Carvalho, P. (2019). Dynamics and functions of lipid droplets. Nat. Rev. Mol. Cell Biol. 20, 137–155. https://doi.org/10.1038/ s41580-018-0085-z.
- Pellegrinelli, V., Carobbio, S., and Vidal-Puig, A. (2016). Adipose tissue plasticity: how fat depots respond differently to pathophysiological cues. Diabetologia 59, 1075–1088. https://doi.org/10.1007/s00125-016-3933-4.
- Petersen, M.C., and Shulman, G.I. (2018). Mechanisms of Insulin Action and Insulin Resistance. Physiol. Rev. 98, 2133–2223. https://doi.org/10. 1152/physrev.00063.2017.
- Kawahito, S., Kitahata, H., and Oshita, S. (2009). Problems associated with glucose toxicity: role of hyperglycemia-induced oxidative stress. World J. Gastroenterol. 15, 4137–4142. https://doi.org/10.3748/wjg.15.4137.
- Blüher, M. (2020). Metabolically Healthy Obesity. Endocr. Rev. 41, bnaa004. https://doi.org/10.1210/endrev/bnaa004.
- Ghaben, A.L., and Scherer, P.E. (2019). Adipogenesis and metabolic health. Nat. Rev. Mol. Cell Biol. 20, 242–258. https://doi.org/10.1038/ s41580-018-0093-z.
- Lecoutre, S., Rebière, C., Maqdasy, S., Lambert, M., Dussaud, S., Abatan, J.B., Dugail, I., Gautier, E.L., Clément, K., and Marcelin, G. (2025). Enhancing adipose tissue plasticity: progenitor cell roles in metabolic health. Nat. Rev. Endocrinol. 21, 272–288. https://doi.org/10.1038/ s41574-024-01071-y.
- Cotillard, A., Poitou, C., Torcivia, A., Bouillot, J.-L., Dietrich, A., Klöting, N., Grégoire, C., Lolmede, K., Blüher, M., and Clément, K. (2014). Adipocyte size threshold matters: link with risk of type 2 diabetes and improved insulin resistance after gastric bypass. J. Clin. Endocrinol. Metab. 99, E1466–E1470. https://doi.org/10.1210/jc.2014-1074.
- Mikkelsen, T.S., Xu, Z., Zhang, X., Wang, L., Gimble, J.M., Lander, E.S., and Rosen, E.D. (2010). Comparative epigenomic analysis of murine and human adipogenesis. Cell 143, 156–169. https://doi.org/10.1016/j.cell. 2010.09.006.
- Lefterova, M.I., Haakonsson, A.K., Lazar, M.a., and Mandrup, S. (2014).
 PPAR gamma and the global map of adipogenesis and beyond. Trends Endocrinol. Metab. 25, 293–302. https://doi.org/10.1016/j.tem.2014. 04.001.

Report



- Smith, U., and Kahn, B.B. (2016). Adipose tissue regulates insulin sensitivity: role of adipogenesis, de novo lipogenesis and novel lipids. J. Intern. Med. 280, 465–475. https://doi.org/10.1111/joim.12540.
- Collins, J.M., Neville, M.J., Pinnick, K.E., Hodson, L., Ruyter, B., van Dijk, T.H., Reijngoud, D.-J., Fielding, M.D., and Frayn, K.N. (2011). De novo lipogenesis in the differentiating human adipocyte can provide all fatty acids necessary for maturation. J. Lipid Res. 52, 1683–1692. https://doi. org/10.1194/jlr.M012195.
- Dunlop, M., and Court, J.M. (1978). Lipogenesis in developing human adipose tissue. Early Hum. Dev. 2, 123–130. https://doi.org/10.1016/ 0378-3782(78)90004-x.
- Couchet, M., Gao, H., Klingelhuber, F., Jalkanen, J., De Castro Barbosa, T., Omar-Hmeadi, M., Massier, L., Krahmer, N., Mejhert, N., and Rydén, M. (2025). Adipogenic characterization of immortalized CD55+ progenitor cells from human white adipose tissue. Adipocyte 14, 2283213. https:// doi.org/10.1080/21623945.2023.2283213.
- Donnelly, K.L., Smith, C.I., Schwarzenberg, S.J., Jessurun, J., Boldt, M.D., and Parks, E.J. (2005). Sources of fatty acids stored in liver and secreted via lipoproteins in patients with nonalcoholic fatty liver disease. J. Clin. Investig. 115, 1343–1351. https://doi.org/10.1172/JCl23621.
- Tang, Y., Wallace, M., Sanchez-Gurmaches, J., Hsiao, W.-Y., Li, H., Lee, P.L., Vernia, S., Metallo, C.M., and Guertin, D.A. (2016). Adipose tissue mTORC2 regulates ChREBP-driven de novo lipogenesis and hepatic glucose metabolism. Nat. Commun. 7, 11365. https://doi.org/10.1038/ ncomms11365.
- Hsiao, W.-Y., and Guertin, D.A. (2019). De Novo Lipogenesis as a Source of Second Messengers in Adipocytes. Curr. Diab. Rep. 19, 138. https:// doi.org/10.1007/s11892-019-1264-9.
- Green, C.R., Wallace, M., Divakaruni, A.S., Phillips, S.A., Murphy, A.N., Ciaraldi, T.P., and Metallo, C.M. (2016). Branched-chain amino acid catabolism fuels adipocyte differentiation and lipogenesis. Nat. Chem. Biol. 12, 15–21. https://doi.org/10.1038/nchembio.1961.
- Zaganjor, E., Yoon, H., Spinelli, J.B., Nunn, E.R., Laurent, G., Keskinidis, P., Sivaloganathan, S., Joshi, S., Notarangelo, G., Mulei, S., et al. (2021). SIRT4 is an early regulator of branched-chain amino acid catabolism that promotes adipogenesis. Cell Rep. 36, 109345. https://doi.org/10. 1016/j.celrep.2021.109345.
- Green, C.R., Alaeddine, L.M., Wessendorf-Rodriguez, K.A., Turner, R., Elmastas, M., Hover, J.D., Murphy, A.N., Ryden, M., Mejhert, N., Metallo, C.M., and Wallace, M. (2024). Impaired branched-chain amino acid (BCAA) catabolism during adipocyte differentiation decreases glycolytic flux. J. Biol. Chem. 300, 108004. https://doi.org/10.1016/j. jbc.2024.108004.
- Kazak, L., and Cohen, P. (2020). Creatine metabolism: energy homeostasis, immunity and cancer biology. Nat. Rev. Endocrinol. 16, 421–436. https://doi.org/10.1038/s41574-020-0365-5.
- Rahbani, J.F., Roesler, A., Hussain, M.F., Samborska, B., Dykstra, C.B., Tsai, L., Jedrychowski, M.P., Vergnes, L., Reue, K., Spiegelman, B.M., and Kazak, L. (2021). Creatine kinase B controls futile creatine cycling in thermogenic fat. Nature 590, 480–485. https://doi.org/10.1038/s41586-021-03221-v.
- Rahbani, J.F., Bunk, J., Lagarde, D., Samborska, B., Roesler, A., Xiao, H., Shaw, A., Kaiser, Z., Braun, J.L., Geromella, M.S., et al. (2024).
 Parallel control of cold-triggered adipocyte thermogenesis by UCP1 and CKB. Cell Metab. 36, 526–540.e7. https://doi.org/10.1016/j.cmet. 2024.01.001.
- Bunk, J., Ersin, M., Hussain, M.F., Samborska, B., Guerra-Martinez, M., Soni, D., and Kazak, L. (2025). Creatine kinase B mediates UCP1-independent beige fat thermogenesis via the futile creatine cycle in mice. Mol. Metab. 98, 102193. https://doi.org/10.1016/j.molmet.2025.102193.
- Kazak, L., Chouchani, E.T., Jedrychowski, M.P., Erickson, B.K., Shinoda, K., Cohen, P., Vetrivelan, R., Lu, G.Z., Laznik-Bogoslavski, D., Hasenfuss, S.C., et al. (2015). A creatine-driven substrate cycle enhances energy

- expenditure and thermogenesis in beige fat. Cell *163*, 643–655. https://doi.org/10.1016/j.cell.2015.09.035.
- Maqdasy, S., Lecoutre, S., Renzi, G., Frendo-Cumbo, S., Rizo-Roca, D., Moritz, T., Juvany, M., Hodek, O., Gao, H., Couchet, M., et al. (2022). Impaired phosphocreatine metabolism in white adipocytes promotes inflammation. Nat. Metab. 4, 190–202. https://doi.org/10.1038/s42255-022-00525-9.
- Arner, E., Daub, C.O., Vitting-Seerup, K., Andersson, R., Lilje, B., Drabløs, F., Lennartsson, A., Rönnerblad, M., Hrydziuszko, O., Vitezic, M., et al. (2015). Transcribed enhancers lead waves of coordinated transcription in transitioning mammalian cells. Science 347, 1010–1014. https://doi.org/10.1126/science.1259418.
- Petrus, P., Lecoutre, S., Dollet, L., Wiel, C., Sulen, A., Gao, H., Tavira, B., Laurencikiene, J., Rooyackers, O., Checa, A., et al. (2020). Glutamine Links Obesity to Inflammation in Human White Adipose Tissue. Cell Metab. 31, 375–390.e11. https://doi.org/10.1016/j.cmet.2019.11.019.
- Pan, X., Ye, L., Guo, X., Wang, W., Zhang, Z., Wang, Q., Huang, J., Xu, J., Cai, Y., Shou, X., et al. (2023). Glutamine Production by Glul Promotes Thermogenic Adipocyte Differentiation Through Prdm9-Mediated H3K4me3 and Transcriptional Reprogramming. Diabetes 72, 1574– 1596. https://doi.org/10.2337/db23-0162.
- Lecoutre, S., Maqdasy, S., Rizo-Roca, D., Renzi, G., Vlassakev, I., Alaeddine, L.M., Higos, R., Jalkanen, J., Zhong, J., Zareifi, D.S., et al. (2024). Reduced adipocyte glutaminase activity promotes energy expenditure and metabolic health. Nat. Metab. 6, 1329–1346. https://doi.org/10.1038/s42255-024-01083-y.
- Klingelhuber, F., Frendo-Cumbo, S., Omar-Hmeadi, M., Massier, L., Kakimoto, P., Taylor, A.J., Couchet, M., Ribicic, S., Wabitsch, M., Messias, A.C., et al. (2024). A spatiotemporal proteomic map of human adipogenesis. Nat. Metab. 6, 861–879. https://doi.org/10.1038/ s42255-024-01025-8.
- Zhong, J., Zareifi, D., Weinbrenner, S., Hansen, M., Klingelhuber, F., Nono Nankam, P.A., Frendo-Cumbo, S., Bhalla, N., Cordeddu, L., de Castro Barbosa, T., et al. (2025). adiposetissue.org: A knowledge portal integrating clinical and experimental data from human adipose tissue. Cell Metab. 37, 566–569. https://doi.org/10.1016/j.cmet.2025.01.012.
- Bäckdahl, J., Franzén, L., Massier, L., Li, Q., Jalkanen, J., Gao, H., Andersson, A., Bhalla, N., Thorell, A., Rydén, M., et al. (2021). Spatial mapping reveals human adipocyte subpopulations with distinct sensitivities to insulin. Cell Metab. 33, 1869–1882.e6. https://doi.org/10.1016/j.cmet.2021.07.018.
- Seppet, E.K., and Saks, V.A. (1994). Thyroid hormones and the creatine kinase system in cardiac cells. Mol. Cell. Biochem. 133–134, 299–309. https://doi.org/10.1007/BF01267962.
- Arner, E., Mejhert, N., Kulyté, A., Balwierz, P.J., Pachkov, M., Cormont, M., Lorente-Cebrián, S., Ehrlund, A., Laurencikiene, J., Hedén, P., et al. (2012).
 Adipose tissue microRNAs as regulators of CCL2 production in human obesity. Diabetes 61, 1986–1993. https://doi.org/10.2337/db11-1508.
- 36. Rodriguez, A.-M., Elabd, C., Amri, E.-Z., Ailhaud, G., and Dani, C. (2005). The human adipose tissue is a source of multipotent stem cells. Biochimie 87, 125–128. https://doi.org/10.1016/j.biochi.2004.11.007.
- Yore, M.M., Syed, I., Moraes-Vieira, P.M., Zhang, T., Herman, M.A., Homan, E.A., Patel, R.T., Lee, J., Chen, S., Peroni, O.D., et al. (2014). Discovery of a class of endogenous mammalian lipids with anti-diabetic and anti-inflammatory effects. Cell 159, 318–332. https://doi.org/10. 1016/j.cell.2014.09.035.
- Uyeda, K., and Repa, J.J. (2006). Carbohydrate response element binding protein, ChREBP, a transcription factor coupling hepatic glucose utilization and lipid synthesis. Cell Metab. 4, 107–110. https://doi.org/10.1016/ j.cmet.2006.06.008.
- Herman, M.A., Peroni, O.D., Villoria, J., Schön, M.R., Abumrad, N.A., Blüher, M., Klein, S., and Kahn, B.B. (2012). A novel ChREBP isoform in adipose tissue regulates systemic glucose metabolism. Nature 484, 333–338. https://doi.org/10.1038/nature10986.



- Dentin, R., Langin, D., and Postic, C. (2012). Hidden variant of ChREBP in fat links lipogenesis to insulin sensitivity. Cell Metab. 15, 795–797. https:// doi.org/10.1016/j.cmet.2012.05.007.
- Li, M.V., Chang, B., Imamura, M., Poungvarin, N., and Chan, L. (2006). Glucose-dependent transcriptional regulation by an evolutionarily conserved glucose-sensing module. Diabetes 55, 1179–1189. https:// doi.org/10.2337/db05-0822.
- Zhang, D., Li, J., Wang, F., Hu, J., Wang, S., and Sun, Y. (2014).
 2-Deoxy-D-glucose targeting of glucose metabolism in cancer cells as a potential therapy. Cancer Lett. 355, 176–183. https://doi.org/10. 1016/j.canlet.2014.09.003.
- Ponticos, M., Lu, Q.L., Morgan, J.E., Hardie, D.G., Partridge, T.A., and Carling, D. (1998). Dual regulation of the AMP-activated protein kinase provides a novel mechanism for the control of creatine kinase in skeletal muscle. EMBO J. 17, 1688–1699. https://doi.org/10.1093/ emboj/17.6.1688.
- Steinberg, G.R., and Hardie, D.G. (2023). New insights into activation and function of the AMPK. Nat. Rev. Mol. Cell Biol. 24, 255–272. https://doi. org/10.1038/s41580-022-00547-x.
- Samborska, B., Roy, D.G., Rahbani, J.F., Hussain, M.F., Ma, E.H., Jones, R.G., and Kazak, L. (2022). Creatine transport and creatine kinase activity is required for CD8+T cell immunity. Cell Rep. 38, 110446. https://doi.org/ 10.1016/j.celrep.2022.110446.
- Sengupta, S., Peterson, T.R., and Sabatini, D.M. (2010). Regulation of the mTOR complex 1 pathway by nutrients, growth factors, and stress. Mol. Cell 40, 310–322. https://doi.org/10.1016/j.molcel.2010.09.026.
- Sabatini, D.M., Erdjument-Bromage, H., Lui, M., Tempst, P., and Snyder, S.H. (1994). RAFT1: a mammalian protein that binds to FKBP12 in a rapamycin-dependent fashion and is homologous to yeast TORs. Cell 78, 35–43. https://doi.org/10.1016/0092-8674(94)90570-3.
- Brown, E.J., Albers, M.W., Shin, T.B., Ichikawa, K., Keith, C.T., Lane, W.S., and Schreiber, S.L. (1994). A mammalian protein targeted by G1-arresting rapamycin-receptor complex. Nature 369, 756–758. https://doi.org/10. 1038/369756a0.
- Kimball, S.R., and Jefferson, L.S. (2006). Signaling pathways and molecular mechanisms through which branched-chain amino acids mediate translational control of protein synthesis. J. Nutr. 136, 227S– 231S. https://doi.org/10.1093/jn/136.1.227S.
- Laplante, M., and Sabatini, D.M. (2012). mTOR signaling in growth control and disease. Cell 149, 274–293. https://doi.org/10.1016/j.cell. 2012.03.017.
- He, L., Lin, J., Lu, S., Li, H., Chen, J., Wu, X., Yan, Q., Liu, H., Li, H., and Shi, Y. (2024). CKB Promotes Mitochondrial ATP Production by Suppressing Permeability Transition Pore. Adv. Sci. 11, e2403093. https://doi.org/10. 1002/advs.202403093.
- Wang, Z., Hulsurkar, M., Zhuo, L., Xu, J., Yang, H., Naderinezhad, S., Wang, L., Zhang, G., Ai, N., Li, L., et al. (2021). CKB inhibits epithelialmesenchymal transition and prostate cancer progression by sequestering and inhibiting AKT activation. Neoplasia 23, 1147–1165. https://doi.org/ 10.1016/j.neo.2021.09.005.
- Hirai, H., Sootome, H., Nakatsuru, Y., Miyama, K., Taguchi, S., Tsujioka, K., Ueno, Y., Hatch, H., Majumder, P.K., Pan, B.-S., and Kotani, H. (2010). MK-2206, an allosteric Akt inhibitor, enhances antitumor efficacy by standard chemotherapeutic agents or molecular targeted drugs in vitro and in vivo. Mol. Cancer Ther. 9, 1956–1967. https://doi.org/10. 1158/1535-7163.MCT-09-1012.
- Whiteman, E.L., Cho, H., and Birnbaum, M.J. (2002). Role of Akt/protein kinase B in metabolism. Trends Endocrinol. Metab. 13, 444–451. https:// doi.org/10.1016/s1043-2760(02)00662-8.
- Vishvanath, L., and Gupta, R.K. (2019). Contribution of adipogenesis to healthy adipose tissue expansion in obesity. J. Clin. Investig. 129, 4022–4031. https://doi.org/10.1172/JCI129191.

- Kim, J.B., and Spiegelman, B.M. (1996). ADD1/SREBP1 promotes adipocyte differentiation and gene expression linked to fatty acid metabolism. Genes Dev. 10, 1096–1107. https://doi.org/10.1101/gad.10.9.1096.
- Ameer, F., Scandiuzzi, L., Hasnain, S., Kalbacher, H., and Zaidi, N. (2014).
 De novo lipogenesis in health and disease. Metabolism 63, 895–902. https://doi.org/10.1016/j.metabol.2014.04.003.
- Deminice, R., da Silva, R.P., Lamarre, S.G., Brown, C., Furey, G.N., McCarter, S.A., Jordao, A.A., Kelly, K.B., King-Jones, K., Jacobs, R.L., et al. (2011). Creatine supplementation prevents the accumulation of fat in the livers of rats fed a high-fat diet. J. Nutr. 141, 1799–1804. https:// doi.org/10.3945/jn.111.144857.
- Deminice, R., de Castro, G.S.F., Francisco, L.V., da Silva, L.E.C.M., Cardoso, J.F.R., Frajacomo, F.T.T., Teodoro, B.G., Dos Reis Silveira, L., and Jordao, A.A. (2015). Creatine supplementation prevents fatty liver in rats fed choline-deficient diet: a burden of one-carbon and fatty acid metabolism. J. Nutr. Biochem. 26, 391–397. https://doi.org/10. 1016/j.jnutbio.2014.11.014.
- He, L., Cho, S., and Blenis, J. (2025). mTORC1, the maestro of cell metabolism and growth. Genes Dev. 39, 109–131. https://doi.org/10.1101/gad. 352084 124
- Yeh, W.C., Bierer, B.E., and McKnight, S.L. (1995). Rapamycin inhibits clonal expansion and adipogenic differentiation of 3T3-L1 cells. Proc. Natl. Acad. Sci. USA 92, 11086–11090. https://doi.org/10.1073/pnas.92. 24.11086.
- Bell, A., Grunder, L., and Sorisky, A. (2000). Rapamycin inhibits human adipocyte differentiation in primary culture. Obes. Res. 8, 249–254. https://doi.org/10.1038/oby.2000.29.
- Gagnon, A., Lau, S., and Sorisky, A. (2001). Rapamycin-sensitive phase of 3T3-L1 preadipocyte differentiation after clonal expansion. J. Cell. Physiol. 189, 14–22. https://doi.org/10.1002/jcp.1132.
- 64. Kim, J.E., and Chen, J. (2004). regulation of peroxisome proliferator-activated receptor-gamma activity by mammalian target of rapamycin and amino acids in adipogenesis. Diabetes 53, 2748–2756. https://doi.org/10.2337/diabetes.53.11.2748.
- Um, S.H., Frigerio, F., Watanabe, M., Picard, F., Joaquin, M., Sticker, M., Fumagalli, S., Allegrini, P.R., Kozma, S.C., Auwerx, J., and Thomas, G. (2004). Absence of S6K1 protects against age- and diet-induced obesity while enhancing insulin sensitivity. Nature 431, 200–205. https://doi.org/ 10.1038/nature02866.
- Le Bacquer, O., Petroulakis, E., Paglialunga, S., Poulin, F., Richard, D., Cianflone, K., and Sonenberg, N. (2007). Elevated sensitivity to dietinduced obesity and insulin resistance in mice lacking 4E-BP1 and 4E-BP2. J. Clin. Investig. 117, 387–396. https://doi.org/10.1172/JCl29528.
- Manning, B.D., and Cantley, L.C. (2007). AKT/PKB signaling: navigating downstream. Cell 129, 1261–1274. https://doi.org/10.1016/j.cell.2007. 06.009.
- Manning, B.D., and Toker, A. (2017). AKT/PKB Signaling: Navigating the Network. Cell 169, 381–405. https://doi.org/10.1016/j.cell.2017.04.001.
- Harrington, L.S., Findlay, G.M., and Lamb, R.F. (2005). Restraining Pl3K: mTOR signalling goes back to the membrane. Trends Biochem. Sci. 30, 35–42. https://doi.org/10.1016/j.tibs.2004.11.003.
- Wueest, S., Schoenle, E.J., and Konrad, D. (2012). Depot-specific differences in adipocyte insulin sensitivity in mice are diet- and function-dependent. Adipocyte 1, 153–156. https://doi.org/10.4161/adip.19910.
- Mileti, E., Kwok, K.H.M., Andersson, D.P., Mathelier, A., Raman, A., Bäckdahl, J., Jalkanen, J., Massier, L., Thorell, A., Gao, H., et al. (2021). Human White Adipose Tissue Displays Selective Insulin Resistance in the Obese State. Diabetes 70, 1486–1497. https://doi.org/10.2337/db21-0001.
- Samaras, K., Botelho, N.K., Chisholm, D.J., and Lord, R.V. (2010). Subcutaneous and visceral adipose tissue gene expression of serum adipokines that predict type 2 diabetes. Obes. Silver Spring Md 18, 884–889. https://doi.org/10.1038/oby.2009.443.

Report



- Song, M.-G., Lee, H.-J., Jin, B.-Y., Gutierrez-Aguilar, R., Shin, K.-H., Choi, S.-H., Um, S.H., and Kim, D.-H. (2016). Depot-specific differences in angiogenic capacity of adipose tissue in differential susceptibility to diet-induced obesity. Mol. Metab. 5, 1113–1120. https://doi.org/10. 1016/j.molmet.2016.09.001.
- Cawthorn, W.P., and Sethi, J.K. (2008). TNF-alpha and adipocyte biology. FEBS Lett. 582, 117–131. https://doi.org/10.1016/j.febslet.2007.11.051.
- 75. Renzi, G., Vlassakev, I., Hansen, M., Higos, R., Lecoutre, S., Elmastas, M., Hodek, O., Moritz, T., Alaeddine, L.M., Frendo-Cumbo, S., et al. (2025). Epigenetic suppression of creatine kinase B in adipocytes links endoplasmic reticulum stress to obesity-associated inflammation. Mol. Metab. 92, 102082. https://doi.org/10.1016/j.molmet.2024.102082.
- Dobre, M.-Z., Virgolici, B., and Timnea, O. (2025). Key Roles of Brown, Subcutaneous, and Visceral Adipose Tissues in Obesity and Insulin Resistance. Curr. Issues Mol. Biol. 47, 343. https://doi.org/10.3390/ cimb47050343.
- 77. Lazarescu, O., Ziv-Agam, M., Haim, Y., Hekselman, I., Jubran, J., Shneyour, A., Muallem, H., Zemer, A., Rosengarten-Levin, M., Kitsberg, D., et al. (2025). Human subcutaneous and visceral adipocyte atlases uncover classical and nonclassical adipocytes and depot-specific patterns. Nat. Genet. 57, 413–426. https://doi.org/10.1038/s41588-024-02048-3.
- Schauer, N., Steinhauser, D., Strelkov, S., Schomburg, D., Allison, G., Moritz, T., Lundgren, K., Roessner-Tunali, U., Forbes, M.G., Willmitzer, L., et al. (2005). GC-MS libraries for the rapid identification of metabolites in complex biological samples. FEBS Lett. 579, 1332–1337. https://doi. org/10.1016/j.febslet.2005.01.029.
- Hofwimmer, K., de Paula Souza, J., Subramanian, N., Vujičić, M., Rachid, L., Méreau, H., Zhao, C., Dror, E., Barreby, E., Björkström, N.K., et al. (2024). IL-1β promotes adipogenesis by directly targeting adipocyte precursors. Nat. Commun. 15, 7957. https://doi.org/10.1038/s41467-024-51938-x.





STAR*METHODS

KEY RESOURCES TABLE

REAGENT or RESOURCE	SOURCE	IDENTIFIER
Antibodies		
Rabbit IgG-HRP	Sigma-Aldrich	Cat#A9169; RRID: AB_258434
Mouse IgG-HRP	Sigma-Aldrich	Cat#5278; RRID: AB_258232
CKB (for western blot)	Proteintech	Cat#15137-1-AP; RRID:AB_2080878
CKB (for immunofluorescence)	Abcam	Cat#AB151579
CKMT2	Abcam	Cat#AB55963; RRID:AB_2081191
B-Actin	Sigma-Aldrich	Cat#A5441; RRID:AB_476744
P-ACC	Cell Signaling Technology	Cat#3661; RRID:AB_330337
FASN	Cell Signaling Technology	Cat#3180; RRID:AB_2100796
Vinculin	Santa Cruz Antibodies	Cat# sc-73614; RRID: AB_1131294
P-P70S6K	Cell Signaling Technology	Cat#9205; RRID:AB_330944
P70S6K	Cell Signaling Technology	Cat#2708; RRID:AB_390722
P-AKT 308	Cell Signaling Technology	Cat#9275; RRID:AB_329828
P-AKT 473	Cell Signaling Technology	Cat#4060; RRID:AB_2315049
AKT	Cell Signaling Technology	Cat#9272; RRID:AB_329827
P-AMPK	Cell Signaling Technology	Cat#2535; RRID:AB_331250
ChREBP	Novus Biological	Cat#NB400-135; RRID: AB_10002435
Tubulin	Cell Signaling Technology	Cat#2125; RRID:AB 2619646
Calnexin	Cell Signaling Technology	Cat#2679; RRID:AB_2228381
PPARG	Cell Signaling Technology	Cat#2435; RRID:AB_2166051
CEBPA	Cell Signaling Technology	Cat#8178; RRID:AB_11178517
FABP4	Atlas Antibodies	Cat#HPA002188; RRID: AB_1078822
ADIPOQ	Thermo Fisher Scientific	Cat#MA1-054; RRID: AB_557516
PLIN1	Cell Signaling Technology	Cat#9349; RRID:AB_10829911
HSL	Cell Signaling Technology	Cat#4107; RRID:AB_2296900
AMPK	Cell Signaling Technology	Cat#2532; RRID:AB_330331
SREBP1 (for immunofluorescence)	Santa Cruz Antibodies	Cat#sc-365513; RRID: AB_10843812
Donkey anti-Mouse IgG (H + L) Highly Cross-Absorbed Secondary Antibody Alexa Fluor 647	Thermo Fisher Scientific	Cat#A31571; RRID:AB_162542
Goat anti-Rabbit IgG (H + L) Highly Cross-Absorbed Secondary Antibody Alexa Fluor 488	Thermo Fisher Scientific	Cat#A11008; RRID:AB_143165
Gene silencers		
ON-TARGETplus Non-targeting Pool	Dharmacon	Cat#D-001810-01-20
ON-TARGETplus siRNA CKB - Human	Dharmacon	Cat#L-006706-00-0005
ON-TARGETplus siRNA CKMT2 - Human	Dharmacon	Cat#L-006709-00-0005
ON-TARGETplus siRNA MLXIPL - Human	Dharmacon	Cat#L-009253-00-0005
ON-TARGETplus siRNA Ckb - Mouse	Dharmacon	Cat#L-062038-00-0005
Critical Commercial Assays		
Script cDNA Synthesis kit	Bio-Rad	Cat#170-8891
Pierce BCA Protein Assay kit	Thermo Fisher Scientific	Cat#23227
HiScribe T7 ARCA mRNA kit (with tailing)	New England Biolabs (NEB)	Cat#E2060S
Seahorse XF Mito Stress Test	Agilent	Cat#103015-100
Seahorse XF Glycolysis Stress Test	Agilent	Cat#103020-100
Human Total Adiponectin/Acrp30 Quantikine ELISA	R&D systems	Cat#DRP300
Lactate-Glo [™] Assay	Promega	Cat#J5021
		(Continued on next page)



Continued		
REAGENT or RESOURCE	SOURCE	IDENTIFIER
Friglyceride quantification assay-Colorimetric/	Sigma-Aldrich	Cat#MAK266-1KT
ATP Determination Kit	Thermo Fisher Scientific	Cat#A22066
Pierce E-Zinc Reversible Stain kit	Thermo Fisher Scientific	Cat#24582
liScribe T7 ARCA mRNA kit (with tailing)	New England Biolabs (NEB)	Cat#E2060S
JucleoSpin RNA, Mini kit for RNA purification	Macherey-Nagel	Cat#32-740955.250
nvitrogen Neon Transfection System 100μL	ThermoFisher	Cat#10114334
Oneasy Blood & Tissue Kit	Qiagen	Cat#69504
NucleoSpin Gel and PCR Clean-up	Macherey-Nagel	Cat#740609.250
Chemicals, Peptides, and Recombinant Proteins		
DharmaFECT 3 Transfection Reagent	Horizon Discovery	Cat#T-2003-03
MEM 1.0g/L Glucose w/o L-Gln	Lonza	Cat#12-707F
YBR-green Master Mix	Bio-Rad	Cat#1708884
mersham ECL Prime Western Blotting Detection leagent	GE Healthcare	Cat#RPN2232
Blotto Immunoanalytical Grade (Non-Fat Dry Milk)	BioNordika	Cat#B501-0500
DΠ	Sigma-Aldrich	Cat#10197777001
-Mercaptoethanol	Sigma-Aldrich	Cat#M3148-100ML
IIPA buffer	Thermo Fisher Scientific	Cat#89901
GF2 human	Sigma-Aldrich	Cat#F0291
nsulin (liquid, ready to use, 10mg/ml, 5mL)	Sigma-Aldrich	Cat#I9278
3	Sigma-Aldrich	Cat#T6397
ransferrin	Sigma-Aldrich	Cat#T8158
BMX (3-Isobutyl-1-methylxanthin)	Sigma-Aldrich	Cat#I5879
losiglitazone (100 mg)	Cayman Chemicals	Cat#71740
examethasone	Sigma-Aldrich	Cat#D1756
.5% Trypsin/EDTA (10x)	Invitrogen (GIBCO)	Cat#15400-054
enicilline G 10000U/ml/Streptomycine 10000μg/ml	Invitrogen (GIBCO)	Cat#15140-122
IEPES 1M	Invitrogen (GIBCO)	Cat#15630-056
lam's F-12 Nutrient Mix	Invitrogen (GIBCO)	Cat#21765-037
MEM, low glucose, pyruvate (+glutamine)	Invitrogen (GIBCO)	Cat#31885-023
x Laemmli Sample Buffer	Bio-Rad	Cat#1610747
odipy 493/503	Thermo Fisher Scientific	Cat#D3922
loechst	Thermo Fisher Scientific	Cat#34580
yQUANT	Thermo Fisher Scientific	Cat#C7026
-deoxy-D-[1-H3]-glucose	PerkinElmer	Cat#NET328250UC
1-[3-H3]-glucose	PerkinElmer	Cat#NET331C001MC
Slucose Solution	Thermo Fisher Scientific	Cat#A2494001
Optiphase Hisafe 3	PerkinElmer	Cat#1200.437
rierce 16% Formaldehyde (w/v), Methanol-Free	Thermo Fisher Scientific	Cat#28906
F-739	Aobious	Cat#AOB33584
IK-2206 2-HCI	SellekChem	Cat#S1078
-deoxy glucose	Sigma-Aldrich	Cat#D3179-1G
apamycin	Sigma-Aldrich	Cat#R8781-200UL
Precision Plus Protein Blue-Stained Protein Standards 0-250kDa	Bio-Rad	Cat#1610373
ngarose, LE, Analytical Grade	Promega	Cat#V3121
SYBR safe DNA Gel Stain	Thermo Fisher Scientific	Cat#S33102
Complete, EDTA-free Protease Inhibitor Cocktail, ablets in glass vials	Sigma-Aldrich	Cat#5056489001
. ab.oto glado vialo		



Continued		
REAGENT or RESOURCE	SOURCE	IDENTIFIER
PhosSTOP	Sigma-Aldrich	Cat#4906837001
QIAzol lysis reagent	Qiagen	Cat#79306
Creatine phosphate	Roche	Cat#10621714001
Dynabeads Protein G for immunoprecipitation	Thermo Fisher Scientific	Cat#10004D
Dynabeads Protein A for immunoprecipitation	Thermo Fisher Scientific	Cat#10002D
Q5 Hot Start High-Fidelty DNA Polymerase	New England Biolabs (NEB)	Cat#M0493L
Agarose, LE, Analytical Grade	Promega	Cat#V3121
SYBR safe DNA Gel Stain	Thermo Fisher Scientific	Cat#S33102
N1-Methylpseudo-UTP	Saveen Werner	Cat#NU-890L
Seahorse XF 100 mm pyruvate solution	Agilent Technologies	Cat#103578-100
Seahorse XF 200 mm glutamine solution	Agilent Technologies	Cat#103579-100
Seahorse XF 1.0 M glucose solution	Agilent Technologies	Cat#103577-100
Seahorse XF DMEM Medium pH 7.4	Agilent Technologies	Cat#103575-100
Seahorse XF Calibrant Medium pH 7.4	Agilent Technologies	Cat#100840-000
Plasmids	. 19.10.11 . 20.11.15.159.100	
HiFi dCas9 VPR	AddGene	Cat#188510
sgRNA		
ID	Sequences	Source
CKB knock out	GTGGCTGTTGGAGAAGGGCA	Thermo Fischer
CKB CRISPRa 1	GCTGCGCGGGTCCCAGCGA	Thermo Fischer
CKB CRISPRa 1	GGCCTCTGGGCGGAAACTG	Thermo Fischer
CKB CRISPRa 1	GCAGAGGCAAGGGCGTGCGA	Thermo Fischer
Primers for <i>in vitro</i> transcription (IVT)		The me Tiesman
T7-CKB mRNA Fwd	ACACTAATACGACTCACTATAGGG GCCACCGTTCGCCTGCGTCGCTCC	Sigma Aldrich
T7-CKB mRNA Rev	CAGACGCAGGCAGGCCAAAACCCT AGTTTATTTCAGCATCAGCAGTATCT	Sigma Aldrich
T7-dCas9-VPR Fw2	ATATTTCTAATACGACTCACTATAG CTTTTTCGCAACGGGTTTGC	Sigma Aldrich
T7-dCas9-VPR Rv2	AACGAAGCTGTTAAAACAGAGATG TGTCGAAGATGGAC	Sigma Aldrich
Softwares and Algorithms		
GraphPad Prism	v.10.6.0	N/A
R Studio	v.4.1.1	N/A
ImageJ	v.2.0.0	N/A
Deposited data		
Raw and analyzed data	This paper	GEO: GSE307820
qPCR primers	Par	
Fwd CKB	TCATCCAGACAGGCGTGGAC	Sigma Aldrich
Rev CKB	GCTCATCGCTGGGCTTGTAG	Sigma Aldrich
Fwd CKMT2	AGGTGACACCCAACGGCTA	Sigma Aldrich
Rev CKMT2	TGACGGGGTCAAAAAGGTCAG	Sigma Aldrich
Fwd HPRT1	CCTGGCGTCGTGATTAGTGAT	, and the second
		Sigma Aldrich
Rev HPRT1	AGACGTTCAGTCCTGTCCATAA	Sigma Aldrich
Fwd B2M	AAGGACTGGTCTTTCTATCTC	Sigma Aldrich
Rev B2M	GATCCCACTTAACTATCTTGG	Sigma Aldrich
Fwd FASN	AAGGACCTGTCTAGGTTTGATGC	Sigma Aldrich
Rev FASN	TGGCTTCATAGGTGACTTCCA	Sigma Aldrich
Fwd SCD	TTCCTACCTGCAAGTTCTACACC	Sigma Aldrich



Continued		
REAGENT or RESOURCE	SOURCE	IDENTIFIER
Rev SCD	CCGAGCTTTGTAAGAGCGGT	Sigma Aldrich
wd ACLY	ATCGGTTCAAGTATGCTCGGG	Sigma Aldrich
Rev ACLY	GACCAAGTTTTCCACGACGTT	Sigma Aldrich
wd CD36	CTTTGGCTTAATGAGACTGGGAC	Sigma Aldrich
Pev CD36	GCAACAACATCACCACACCA	Sigma Aldrich
wd ACACA	ATGTCTGGCTTGCACCTAGTA	Sigma Aldrich
Rev ACACA	CCCCAAAGCGAGTAACAAATTCT	Sigma Aldrich
wd SLC2A4	TGGGCGGCATGATTTCCTC	Sigma Aldrich
ev SLC2A4	GCCAGGACATTGTTGACCAG	Sigma Aldrich
wd PPARG	TCATAATGCCATCAGGTTTG	Sigma Aldrich
ev PPARG	CTGGTCGATATCACTGGAG	Sigma Aldrich
wd CEBPA	AGCCTTGTTTGTACTGTATG	Sigma Aldrich
ev CEBPA	AAAATGGTGGTTTAGCAGAG	Sigma Aldrich
wd PLIN1	TGGAGACTGAGGAGAACAAG	Sigma Aldrich
ev PLIN1	ATGTCACAGCCGAGATGG	Sigma Aldrich
wd LPL	TCATTCCCGGAGTAGCAGAGT	Sigma Aldrich
ev LPL	GGCCACAAGTTTTGGCACC	Sigma Aldrich
wd ADIPOQ	GGTCTCGAACTCCTGGCCTAA	Sigma Aldrich
ev ADIPOQ	TGAGATATCGACTGGGCATGGT	Sigma Aldrich
wd FABP4	ACTGGGCCAGGAATTTGACG	Sigma Aldrich
ev FABP4	CTCGTGGAAGTGACGCCTT	Sigma Aldrich
wd Fasn	GGAGGTGGTGATAGCCGGTAT	Sigma Aldrich
ev Fasn	TGGGTAATCCATAGAGCCCAG	Sigma Aldrich
wd Scd	TTCTTGCGATACACTCTGGTGC	Sigma Aldrich
ev Scd	CGGGATTGAATGTTCTTGTCGT	Sigma Aldrich
wd Acly	ACCCTTTCACTGGGGATCACA	Sigma Aldrich
ev Acly	GACAGGGATCAGGATTTCCTTG	Sigma Aldrich
wd Cd36	ATGGGCTGTGATCGGAACTG	Sigma Aldrich
lev Cd36	TTTGCCACGTCATCTGGGTTT	Sigma Aldrich
wd Acaca	CTCCCGATTCATAATTGGGTCTG	-
ev Acaca	TCGACCTTGTTTTACTAGGTGC	Sigma Aldrich Sigma Aldrich
wd Slc2a4	ACACTGGTCCTAGCTGTATTCT	-
ev Slc2a4	CCAGCCACGTTGCATTGTA	Sigma Aldrich Sigma Aldrich
		<u> </u>
wd Pparg	CTCCAAGAATACCAAAAGTGCGA	Sigma Aldrich
ev Pparg	GCCTGATGCTTTATCCCCACA CAAGAACAGCAACGAGTACCG	Sigma Aldrich
wd Cebpa	GTCACTGGTCAACTCCAGCAC	Sigma Aldrich
ev Cebpa		Sigma Aldrich
wd Fabp4	AAGGTGAAGAGATCATAACCCT	Sigma Aldrich
ev Fabp4	TCACGCCTTTCATAACACATTCC	Sigma Aldrich
wd Plin1	CTGTGTGCAATGCCTATGAGA	Sigma Aldrich
ev Plin1	CTGGAGGGTATTGAAGAGCCG	Sigma Aldrich
wd Adipoq	TGTTCCTCTTAATCCTGCCCA	Sigma Aldrich
lev Adipoq	CCAACCTGCACAAGTTCCCTT	Sigma Aldrich
wd Ckb	AAGTTCTCGGAGGTGCTCAA	Sigma Aldrich
ev Ckb	CCGTTGCTCCATCTCAATG	Sigma Aldrich
wd Hprt	TCAGTCAACGGGGACATAAA	Sigma Aldrich
Rev Hprt	GGGGCTGTACTGCTTAACCAG	Sigma Aldrich



Continued		
REAGENT or RESOURCE	SOURCE	IDENTIFIER
Fwd Lrp10	GGATCACTTTCCCACGTTCTG	Sigma Aldrich
Rev Lrp10	GAGTGCAGGATTAAATGCTCTGA	Sigma Aldrich
Fwd Elovl3	TACATCTGGAGGCAGGAGAA	Sigma Aldrich
Rev Elovl3	GGTGGAAGAGTGAGCGAATAG	Sigma Aldrich

EXPERIMENTAL MODEL AND SUBJECT DETAILS

Subjects

Human adipose tissue biopsy data were previously characterized and kindly provided by Prof. Mikael Rydén and Dr. Niklas Mejhert (Karolinska Institutet, Stockholm, Sweden), as described in clinical cohort $2^{26,35}$ and spatial transcriptomics cohorts. All studies were approved by the Regional Board of Ethics in Stockholm, as previously published, $2^{6,32,33,35}$ and followed the declaration of Helsinki ethical principles for medical research involving human subjects. Written informed consent was obtained from all subjects.

Cell cultures

Human preadipocyte culture

In vitro differentiated human adipocytes were differentiated from CD55⁺ progenitors and cultured and according to the methodology described in a previous work of our lab.²⁶ In brief, progenitors were isolated from abdominal subcutaneous WAT of one male and one female donor²⁶ and maintained in DMEM containing 10% FBS, 10 mM HEPES, 50 μ g/mL penicillinstreptomycin, and 2.5 ng/mL fibroblast growth factor 2 (FGF). At ~90% confluency, FGF was removed, cells were washed with PBS (pH 7.4), and differentiation was induced for 10 days using an adipogenic cocktail.¹² During differentiation, cells were treated with: phosphocreatine (1–30 mM, 24 h), 2-deoxy-D-glucose (0.1 mM, 48 h), rapamycin (500 nM, 48 h), PF-739 (5 μ M, 48 h), or MK-2206 (10 μ M, 48 h). Low-BCAA medium was generated by replacing DMEM (BCAA 304 mg/L) with F12 medium (BCAA 28.8 mg/L) from day 8 of differentiation for 48 h.

Isolated human primary adipocytes from a male and a female donor were used for cell culture, for transcriptomic analyses, ^{26–28} and for proteomics.³¹ All studies were approved by the Regional Board of Ethics in Stockholm, as previously published, ^{26–28,31} and followed the declaration of Helsinki ethical principles for medical research involving human subjects. Written informed consent was obtained from both subjects.

Human multipotent adipose-derived stem culture

hMADS cells were maintained in low-glucose DMEM supplemented with 10% FBS, 2 mM L-glutamine, 10 mM HEPES, 50 U/mL penicillin, 50 μ g/mL streptomycin, and 2.5 ng/mL human FGF2. Cells were seeded in 6-well plates at 44,000 cells/mL and incubated at 37°C in 5% CO₂. Six days after seeding, FGF2 was removed. On the following day (day 0), differentiation was initiated in serum-free proliferation medium/Ham's F-12 containing 10 μ g/mL transferrin, 5 μ g/mL insulin, 0.2 nM triiodothyronine, 100 μ M 3-isobutyl-1-methylxanthine, 1 μ M dexamethasone, and 100 nM rosiglitazone. At day 3, dexamethasone and 3-isobutyl-1-methylxanthine were omitted from the medium, and at day 9, rosiglitazone was also removed. hMADS were generously provided by Prof. Ez-Zoubir Amri (Université Côte d'Azur, Nice, France).

Murine primary adipocyte culture

Primary adipocytes were isolated from inguinal WAT of female mice fed a standard chow diet. Minced adipose tissue was digested in collagenase-containing medium for 1 h at 37° C under lateral shaking (100 rpm). The suspension was filtered through a 100 μ m strainer, diluted to 30 mL with PBS, pelleted (10 min, 1,500 rpm), and resuspended in 12 mL DMEM containing 10% fetal calf serum. Cells (0.5 mL/well) were plated in 12-well plates and incubated at 37° C in 95% air/5% CO₂. After 4 h, unattached cells were removed by three PBS washes, and cultures were maintained in fresh medium. After three passages, cells were seeded at 20,000 cells/well in 48-well plates. Differentiation was induced with growth medium containing 2% FBS, 1 μ mol/L dexamethasone, 0.5 μ mol/L isobutyl-methylxanthine, 100 nmol/L insulin, and 1 μ mol/L rosiglitazone for 3 days. Medium was then replaced with growth medium containing 2% FBS and 100 nmol/L insulin for 2 days, followed by growth medium with 2% FBS alone for the final 2–3 days of differentiation.

Animal experiments were performed according to procedures approved by the local ethic committee and received permission from the French "Ministère de l'Enseignement Supérieur, de la Recherche et de l'Innovation". All animal procedures were reviewed and approved by local and national comities and conducted in accordance with the Guide for the Care and Use of Laboratory Animals published by the European Commission Directive 86/609/EEC.

Animals

The generation, housing and diet intervention of mice $Ckb^{Adipo-Cre}$ and $Ckb^{fl/fl}$ animals has been previously described.²² Male mice were fed a high fat diet for 6 weeks. WAT was obtained from the epididymal WAT and inguinal WAT depots. Samples for qPCR



analyses were snap-frozen in liquid nitrogen immediately. One part of the fresh tissue samples was fixed in 4% formalin (pH 7.0) and used for immunofluorescence analyses as described below. Samples from these animals were generously provided by Dr. Lawrence Kazak (McGill, Montreal, Canada).

Animal experiments were performed according to procedures approved by the Animal Resource Center at McGill University and complied with guidelines set by the Canadian Council of Animal Care, as previously published.²²

METHOD DETAILS

RNA isolation, cDNA synthesis and real-time qPCR

Total RNA was extracted from cells plated in 48 well plates as described previously. 26 The concentration, purity and quality of RNA were measured using both Nanodrop 2000 (Thermo Fisher) and Agilent 2100 Bioanalyzer (Agilent Technologies). Conversion of RNA in cDNA was made using iScript cDNA synthesis kits (BioRad) and concentration adjusted at $1 \text{ng}/\mu\text{L}$. Expression of mRNA levels by qPCR were then measured using Sybergreen master mix assay, Ct values were then used to calculate relative expression with the comparative Ct-method, i.e., $2^{\Delta\text{Ct-target gene}}/2^{\Delta\text{Ct-reference gene}}$. Primer sequences (mice and human) are listed in the key resources table.

In vitro transcription and mRNA-based re-expression

CKB and Catalytically inactive Cas9 fused with tripartite VPR (dCas9-VPR) mRNA were generated using T7-contaning primers, amplifying the coding sequence contained in cDNA from cells and plasmid vector respectively. Synthesis of mRNA was then performed using HiScribe T7 ARCA mRNA Kit (with tailing) per manufacturer's instructions. To improve stability, N1-Methylpseudo-UTP was incorporated into the mRNA as previously described. ⁷⁵

CRISPRa for endogenous CKB overexpression

mRNA encoding dCas9-VPR was introduced in the cells one day prior to adipogenesis induction with Neon transfection system as previously reported⁷⁵ along with a pool of 3 guides RNA targeting area surrounding CKB transcription start site as listed in the key resources table. Neon transfection conditions utilized to introduce mRNA were the following (1700 V, 20 ms, one pulse).

RNAi and re-expression experiments at D3 and D8

For depletion experiments, siRNA oligonucleotides (final concentration of 20 nM) targeting CKB, MLXIPL or a non-silencing control were introduced to the cells by electroporation (1,300 V, 20 ms, 2 pulses) using the Neon Transfection system, 100 μ L Kit (Invitrogen) at D3 or D8 of differentiation as previously described. For re-expression experiments (see above), mRNA encoding CKB (20 pmol) or a non-coding control was introduced in the same manner by the Neon Transfection system, 100 μ L Kit, (1,300 V, 20 ms, 2 pulses). Cells were then seeded in plates and incubated with the differentiation medium containing adipogenic cocktail until full differentiation. The gene silencing references are listed in the key resources table.

Early transfection of pre-adipocytes (D-1) and incubations with chemicals

Early transfection of pre-adipocytes was performed one day prior to beginning of differentiation. Transfection media was prepared using Pure DMEM Medium, siRNA (non-targeting control, *CKB*, *CKMT2*, 40 nM final concentration) and Dharmafect 3. Hence, the mixture was plated and incubated at room temperature for 30 min before adding cells resuspended in proliferation media at a concentration of 250 cells/µL without FGF. After 24 h cells were washed once with 1x PBS and differentiation cocktail added on cells. When required, cells were trypsinized at day 8 (D8) and transfected again with siRNA targeting *MLXIPL*, *CKB*, or non-silencing control as described above. At day 10 (D10), cells were treated with the indicated chemical compounds.

Library preparation and RNA sequencing

In brief, 100 ng of isolated total RNA from siC, siCKB and siCKMT2 cells were used for library preparation. The quality and yield of the samples were assessed using Qubit (Thermo Fisher) and Tape station (Agilent), thereafter normalized and combined. These pools were sequenced on the Illumina Nextseq 2000 p2 100 cycles sequencing run, generating 59 base single ends read with dual index. Base scalling and demultiplexing was performed using CASAVA software with default settings generating Fastq files aligned to GRCh38 for further downstream mapping and analysis. Raw counts were normalized and analyzed using DESeq2 in R studio (v4.1.1). Pathway analyses were performed using KEGG Human 2021 annotations. Plotting of omics data was performed with ggplot2 and ggigraph. The data is deposited in GEO under the accession GEO number GSE307820.

Western Blot analysis

Western blotting was performed as previously described.²⁶ All antibodies are listed in the key resources table. For protein of interest located at the same size, lysates were subdivided in equal amounts and loaded on separate gels.

Immunoprecipitation from whole lysate

Adipocytes were seeded and differentiated in 15 cm² dishes. At D10 post-induction, cells were washed three times in ice-cold PBS followed by one wash with immunoprecipitation (IP) base buffer (10 mM Tris-HCl, pH 7.5; 150 mM NaCl; 0.5 mM EDTA). Cells were





then lysed in 400 μ L of IP lysis buffer (base buffer supplemented with 0.5% NP-40, protease inhibitor cocktail, and phosphatase inhibitor) and collected into 1.5 mL Eppendorf tubes. Lysates were incubated on ice for 30 min with gentle resuspension every 10 min. Following lysis, samples were centrifuged at 17,000×g for 20 min at 4°C. The resulting supernatant was carefully transferred to a new tube, avoiding both the pellet and upper lipid layer, and diluted with 600 μ L of dilution buffer (base buffer supplemented with protease and phosphatase inhibitors).

An aliquot of 100 μ L was removed and stored as input control for subsequent western blot analysis. The remaining lysate was incubated overnight at 4°C on a rotating platform with 3 μ g of antibody (AKT or control IgG). The following day, protein A and G magnetic beads were calibrated separately for 15 min and then combined (30 μ L each per reaction). Beads were added to the antibody-incubated lysates and rotated for an additional 3 h at 4°C to ensure binding.

After incubation, the depleted supernatant was collected and stored. Beads were washed five times in wash buffer (base buffer containing 0.05% NP-40, protease and phosphatase inhibitors), followed by a final wash in ice-cold PBS. Proteins were eluted by resuspending beads in 30 µL of elution buffer (22.5 µL RIPA, 7.5 µL 4x Laemmli sample buffer, 1 mM DTT, protease and phosphatase inhibitors) and incubated at 95°C for 10 min. Eluted proteins and input controls were resolved by SDS-PAGE for immunoblot analysis.

ATP measurement

Measures of cellular ATP levels were performed in cell lysates per manufacturer's instructions. Per well in a 96-well plate, 10,000 to 15,000 cells were seeded at D-1 after transfection with siRNA directed against control or CKB. The assay was performed at D10 post differentiation with the adipogenic cocktail. Data were normalized by protein levels.

Metabolomic samples preparation and targeted metabolomic measurements

Cells were plated in 15 cm² dishes and differentiated up to day 10. Thereafter, cells were washed in cold PBS twice, then scraped in ice-cold 90% methanol, collected and snap frozen in liquid nitrogen. Metabolites extraction and mass spectrometry analysis were carried out as previously described. ^{26,30} Metabolites were profiled at the Swedish Metabolomics Center. The cell extracts were split in 3 parts and analyzed by (i) gas chromatography-mass spectrometry (GC-MS) to target TCA metabolites after derivatization, (ii) hydrophilic interaction liquid chromatography-mass spectrometry (HILIC-MS) to target nucleotides, creatine, and other phosphorylated metabolites after reconstitution of the dried extract in 50 µL of 50% methanol, and (iii) LC-MS to target amino acids after derivatization of the dried extract with AccQ-Tag reagent. The metabolites were annotated by library matching of their retention index (GC-MS) and retention time (LC-MS) and their exact mass. ⁷⁸ Mass spectra and retention index comparison from GC-MS analyses was performed using NIST MS v.2.2 software. Both the Swedish Metabolomics Center's in-house standards libraries and public libraries as NIST (https://chemdata.nist.gov/) and MoNA (https://mona.fiehnlab.ucdavis.edu/) were used. The 13C-label-ling was calculated by using an in-house script.

Creatine kinase activity

Creatine kinase activity was measured following the manufacturer's instructions. Briefly, cells were seeded on D–1 at a density of 5×10^6 per well in 6-well plates after transfection with either control siRNA (siC) or CKB-targeting siRNA (siCKB). The assay was performed on day 10 of differentiation. Cells were lysed in 200 μ L homogenization buffer (250 mM sucrose, 1 mM Tris-HCl pH 7.4, 1 mM EDTA pH 8, 2% BSA) and passed through a 23 G needle more than 15 times. Lysates were centrifuged at 20,000 \times g for 40 min at 4°C, and the supernatant (cytosolic fraction) was collected. Creatine kinase activity was determined using 10 μ L of the cytosolic fraction, according to the manufacturer's protocol. Total protein concentration was measured for normalization, and background signal from siCKB samples was subtracted from all measurements.

ELISA assays

Adiponectin and lactate quantification in cultured media of cells harvested at D10 were performed according to manufacturer instructions. Data obtained were normalized by RNA concentration per well.

Triglyceride extraction and measurement

In brief, cells seeded in 96-well plates, plated at the density of 15,000 cells/well. At D10 of differentiation, triglyceride extraction was performed by using 5% NP40 and employing the Triglyceride Quantification Colorimetric/Fluorometric Kit, following manufacturer instructions.

Immunofluorescence (IF)

Murine WAT samples were fixed in 4% PFA for 24 h at 4°C, embedded in paraffin, and sectioned at 5 µm thickness. Sections were stained with hematoxylin and eosin (H&E, Sigma-Aldrich) following standard protocols. For immunofluorescence, sections were incubated overnight at 4°C with either SREBP1 antibody (1:50) or anti-CKB antibody (1:100). Detection was performed using anti-rabbit Alexa Fluor 488 (1:500) for CKB or anti-rabbit Alexa Fluor 647 (1:500) for SREBP1, applied for 1 h at room temperature. Nuclear counterstaining was done with Hoechst (1:500) for 20 min at room temperature. Quantification of SREBP1-positive cells was carried out in ImageJ by measuring SREBP1 signal intensity in 3 randomly selected fields per section at 20× magnification using an Axio Observer.Z1 inverted fluorescence microscope (Zeiss) with AxioVision software, normalizing total intensity to Hoechst signal.



Confocal microscopy

Images were acquired using a Nikon multipoint spinning disk confocal inverted microscope, equipped with a Kinetix sCMOS camera $(6.5 \, \mu m \, \text{pixel size})$. Imaging was performed with 10x, 20x, and $40 \times \text{air objectives}$ to capture a range of magnifications suitable for the experimental setup.

Quantification of lipid accumulation (by Bodipy staining)

Cells cultured in 96-well plates were fixed with 4% paraformaldehyde for 10 min at room temperature. Following fixation, they were washed three times with PBS and then stained for 20 min at room temperature with Hoechst 33342 (2 μ g/mL, #H3570) and BODIPY 493/503 (0.2 μ g/mL, #D3922), both supplied by Invitrogen (Thermo Fisher Scientific). After staining, the cells were washed three additional times with PBS. Imaging was carried out using a 10× objective on the CellInsight CX5 high-content screening system (Thermo Fisher Scientific), following a previously reported protocol. Quantification of nuclei and lipid droplets was performed using the object and spot detection algorithms provided in the HCS Studio: Cellomics Scan software (v6.6.0, Thermo Fisher Scientific), with border nuclei automatically excluded. The lipid droplet area per cell was calculated by dividing the total lipid droplet area in a well by the number of nuclei in that same well.⁷⁹

Seahorse assays

OCR and ECAR were measured with XF96 Seahorse Extracellular Flux Analyzer (Agilent) using Cell Mito Stress and Cell Glyco Stress Test Kits as previously described²⁶. For Mito Stress Test, cells were incubated in medium supplemented with 1 mM pyruvate, 2 mM glutamine and 10 mM glucose for 1 h. Mito Stress assays were performed by sequential addition of 1.5 μM oligomycin (inhibitor of ATP synthesis), 1.5 μM FCCP and 0.5 μM rotenone/antimycin A (inhibitors of complex I and complex III of the respiratory chain, respectively). For Glyco Stress Test, cells were incubated in medium supplemented with 2 mM glutamine for 1 h. Glyco Stress assays were performed by sequential addition of glucose 100 mM, 1.5 μM oligomycin (inhibitor of ATP synthesis) and 2-DG 500 mM. Immediately after the assay, cells were incubated with CyQUANT Kit reagent and fluorescence was measured for data normalization. Fluorescence was quantified using Varioskan LUX (Thermo Fisher Scientific) according to manufacturer instructions.

Radioactive de novo lipogenesis measurement

Cells were sensitized to insulin with 1/20 reduction 48 h prior to experiment, 24 h later insulin was completely removed. The day of the experiment cells were then incubated with media containing 3 H-glucose (0.1 μ M) with and without insulin (150 nM) for 2 h. Cells were then lysed in 0.1% SDS (in H₂O) and the lysates resuspended in 4 mL toluene overnight. Radioactivity was quantified using a beta counter. A portion of each lysate was reserved for protein quantification to normalize DNL measurements.

Radioactive glucose uptake measurement

Cells were sensitized to insulin with 1/20 reduction 48 h prior to experiment, 24 h later insulin was completely removed. On the day of the experiment cells were then incubated with media containing 2-deoxy-D-[1H 3]-glucose (0.5 μ M) with and without insulin (150 nM) for 40 min. Cells were then washed twice with cold PBS then lysed in 0.1% SDS/H $_2$ O RIPA buffer and resuspended in Optiphase HiSafe for at least 3 h prior to beta counter measurement. Portion of lysate was used for protein quantification using Pierce BCA Protein determination kit (ThermoFisher) for normalization. The rest of the lysate was transferred to cuvettes containing scintillation fluid and counts per minute was recorded using a Liquid Scintillation Analyser (Tri-Carb 4910 TR, PerkinElmer).

QUANTIFICATION AND STATISTICAL ANALYSIS

Data are reported as mean with SEM unless otherwise stated. Results were compared by Student t-test, One- or Two-way analysis of variance (ANOVA) with Dunnett's or Tukey's post-hoc tests respectively. For correlation analyses in clinical cohorts, simple and multiple regression analyses (with BMI included as independent regressor) were used. Statistical analyses were performed using Prism (GraphPad Software) and bioinformatic analyses using R v.4.1.1.